Unveiling the Pool of Metallophores in Native Environments and Correlation with Their Potential Producers

Francisco Calderón Celis, Ivan González-Álvarez, Magdalena Fabjanowicz, Simon Godin, Laurent Ouerdane, Béatrice Lauga, Ryszard Lobinski

Unveiling the pool of metallophores in native environments and correlation to their potential producers

Francisco Calderón Celis[1*$], Ivan González-Álvarez[1], Magdalena Fabjanowicz[2], Simon Godin[1], Laurent Ouerdane[1], Béatrice Lauga[1], Ryszard Łobiński[1,3]

[1]Universite de Pau et des Pays de l'Adour, E2S UPPA, CNRS, IPREM, Pau, France

[2]Gdańsk University of Technology, Faculty of Chemistry, Department of Analytical Chemistry, ul. G. Narutowicza 11/12, 80-233 Gdańsk, Poland

[3]Chair of Analytical Chemistry, Warsaw University of Technology, 00-664 Warsaw, Poland

*Authors to whom correspondence should be addressed:

Email: calderonfrancisco@uniovi.es

Institute of Analytical Sciences and Physico-Chemistry for Environment and Materials, Universite de Pau et des Pays de l'Adour, Pau, France.

[$]*Current address: Department of Physical and Analytical Chemistry, University of Oviedo, Oviedo, Spain.*

Abstract

For many organisms, metallophores are essential biogenic ligands that ensure metals scavenging and acquisition from their environment. Their identification is highly challenging in highly organic matter rich environments like peatlands, due to low solubilization and metal scarcity, and high matrix complexity. In contrast to common approaches based on sample modification by spiking of metal isotope tags, we have developed a 2D SPE-LC-MS approach for the high-sensitive (LOD 40 fmol per g of soil), high-resolution direct detection and identification of metallophores in both their non-complexed (apo) and metal complexed forms in native environments. The characterization of peat collected in Bernadouze (France) peatland resulted in the identification of 53 metallophores by database mass-based search, 36 among which are bacterial. Furthermore, detection of the characteristic (natural) metal isotope patterns in MS resulted in the detection of both Fe and Cu potential complexes. A taxonomic-based inference method was implemented based on literature and public databases (antiSMASH database version 3.0) searches allowing to associate over 40% of the identified bacterial metallophores with potential producers. In some case low completeness with the MIBiG reference BCG might be indicative of alternative producers in the ecosystem. Thus, coupling of metallophores detection and producers' inference could pave a new way to investigate poorly documented environment searching for new metallophores and their producers yet unknown.

Keywords

Mass spectrometry, SPE-LC-MS, Metallophores, Siderophores, Peatlands, Microbial community.

Graphical Abstract

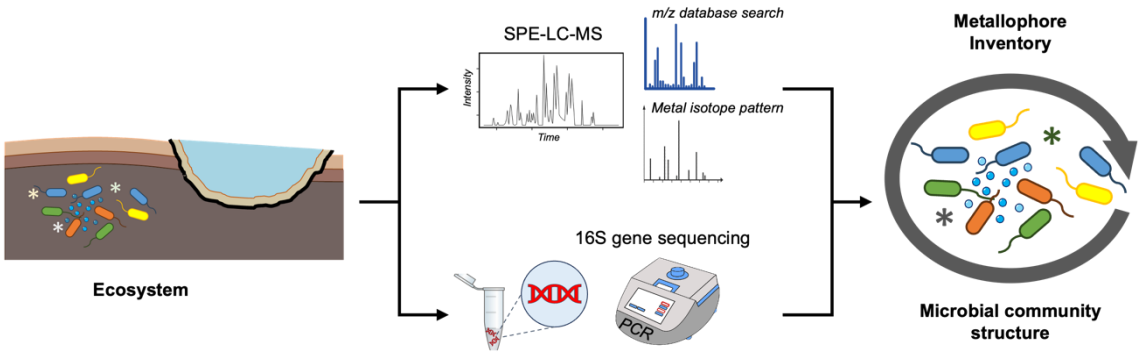

Synopsis

The characterization of the metallophores pool in native environments remains a challenge. This study reports tens of metallophores in peatland soil and the association with potential microbial producers.

1. INTRODUCTION

Metallophores are organic ligands produced by bacteria, fungi and plants that scavenge metals from the environment (terrestrial and marine) creating a soluble complex.[1,2] They play a pivotal role in metal homeostasis, making the metal available to the cell, or contributing to the mitigation of toxic metals contamination from the environment.[3–6] The former has great repercussions e.g. in agriculture, making the metals more available to the plant promoting its growth,[7] whereas the latter has great impact in environmental bioremediation.[8,9] In condition of metal scarcity, the production of metallophores by some microorganisms could participate in shaping microbial communities by promoting both cooperative and competitive interactions.[10,11] Among metallophores, the best-known and studied are those that complex iron, also known as siderophores.[12,13] Siderophores produced by bacteria and fungi that thrive at neutral pH (ideal conditions for binding) are well characterized, with hundreds of them identified, mostly using laboratory incubation cultures.[1,14] However, in the case of soils and environments rich in organic matter, iron availability is constricted, becoming growth limiting. The limited recovery of siderophores from the environment as well as the alkalinity and complexity of the matrix make the identification of siderophores (and other metallophores by extension) in these environments highly challenging.[14]

Whereas commonly used colorimetric methods (e.g., Chrome Azurol S) provide information on the formation of metal-complex, and in some cases have enough specificity to discriminate between catecholate or hydroxamate siderophores,[15] identification of metallophores requires high-resolution mass spectrometry approaches. The most common strategy is the use of metal-induced isotope pattern.[16] That is, the sample is spiked with a solution containing two isotopes of each metal, so that when the metallophore complexes both isotopes, the resulting species will have a specific mass difference and intensity ratio that can be searched for in the mass spectra to detect organic ligands that complex the metal. This strategy is eventually conditioned by the

complexation capacity of all metallophores in the sample, as well as the alteration of the natural environment of the sample, losing its representativity.

Herein we conduct an alternative approach for the identification of metallophores in peat based on an analytical platform that combines online sample enrichment coupled to high resolution MS. Peat soils are mostly made of organic matter as the result of plant decomposition, resulting in being very rich in organic matter but poor in minerals.[17] The proposed approach is applicable directly to the non-altered environmental sample, and provides the required conditions of siderophores recovery, methodological sensitivity, and data quality to detect high- and low-abundant metallophores through their mass and the characteristic natural isotope pattern of metal complexes. In addition, we also developed an inference approach relying on the taxonomic profile of the prokaryotic community and the mining of the antiSMASH database to link metallophores to potential producers in the peat.

2. MATERIAL AND METHODS

2.1. Peat collection and treatment

Peat was collected in the Bernadouze peatland (Ariège, France) on 19/09/2019. A core of 50 cm depth was retrieved using a Russian corer in an ombrotrophic area in a lawn microform. The core was stored at 4ºC until processing. The sample border was removed to avoid trace metal contamination from the corer. Water extraction was performed to extract siderophores from peat sample in a 1:10 ratio MilliQ grade water, adapted from Boiteau et al.[18] Briefly, mixture was vigorously shaken in plastic Falcon® 50 ml tubes at room temperature for 10 min until sample homogenization before collection. Water extract was centrifuged during 10 min at 4500 rpm at 4ºC, and the supernatant was filtered using Millex-HP 0.22 µm Syringe Filter, polyethersulfone (Merck). Filtered samples were stored at -20ºC until analyzed.

2.2. DNA extraction, 16S rDNA sequencing and sequences treatment

DNA was extracted from the peat using the DNeasy Powersoil Pro Kit (QIAGEN®). The 16S rDNA gene was amplified by PCR using the Bacteria/Archaea 16 rDNA primers 515F (5´-GTGYCAGCMGCCGCGGTA-3´) and 928R (5´-CCCCGYCAATTCMTTTRAGT-3´). PCR was conducted in technical triplicates according to the following program: 95ºC for 10 min and 32 cycles of 95ºC for 30s, 60ºC for 30s, and 72°C for 40s, followed from a final extension of 72ºC for 10 min. Amplicons were sequenced by Platform Genome Transcriptome of Bordeaux (PGTB) using NGS Illumina MiSeq (version v3). Sequence data was analyzed using the QIIME2 version 2021.4.[19] The raw sequences were denoised with DADA2[20] to construct error-corrected amplicon sequence variants (ASVs). ASVs taxonomical assignation was performed against SILVA database (release 138.1) (Quast et al., 2013)[21] via q2-feature-classifier.[22]

2.3. SPE-LC-MS analysis of peat extract

Online solid phase extraction (SPE) was used to carry out sample clean-up and preconcentration (Fig S1), followed by liquid chromatography separation (LC) and high-resolution mass spectrometry (MS) detection using electrospray (ESI) with orbitrap analyzer (Fig 1) (conditions in Supporting Information, SI). Parallel SPE-LC-ICP-MS detection provided profiling of potentially metallophores metal complexes. Siderophores target detection was done through mass comparison with online databases. The characteristic isotope pattern of common metals complexed to these metallophores would be searched for untargeted detection in the acquired mass spectra during the analyses. Abundance estimation of identified siderophores in Bernadouze peatland was done using calibration curves build for the 7 siderophores standards spiked at different concentrations ranging from 0 to 1 nmol/mL in the sample (Fig S2). Differences in ionization efficiency depending on siderophores structure or matrix effects were addressed by averaging the calibration curves.

2.4. Prediction of siderophore producers

The prediction of siderophore producers was inferred by coupling taxonomic information obtained from 16S rRNA gene sequences and metallophores inventories obtained by mass spectrometry. Two different approaches were performed: i) using the Siderophore base (http://bertrandsamuel.free.fr) along a literature search (Web of Science and PubMed); ii) mining the antiSMASH database version 3 (Fig S3). The literature search was conducted to both identify taxa known to produce any MS-detected siderophore in our sample and taxa known to occur in peatlands.

The antiSMASH database consists in a collection of annotated BGC from 25236 bacterial, 388 archaean and 177 fungal genomes cross-referenced with the MIBiG curated database.[23] We retrieved all siderophore secondary metabolite cluster entries (7909) knowing that these only cover siderophore BGCs that included IucA/IucC biosynthetic gene family.[24] This siderophore database contains all potential siderophore producers including their taxonomy (Genus, species, strain) along with the genome NCBI accession number, the region of the genome containing the BGC, the position of the BGC in the contig (edge and not), the most similar known BGC (i.e. the name of the siderophore), the percentage of similarity to the closest MIBiG BGC, the identifier of this MIBiG BGC and the antiSMASH URL. Among the whole siderophore entries, 2343 entries lacked the three penultimate pieces of information (either labeled as "none" or empty). Overall, this database covered 487 genus, 1792 species and 3888 strains and 143 siderophore types with BGC completeness (percentage of conserved genes) ranging from 1 to 100% as compared to the MIBiG reference BGC. The antiSMASH siderophore database was then filtered against the peat taxons (16S based prokaryotic community composition) at the genera level using the *dplyr* R package[25] to identify the potential siderophore producers in the peat sample. This information was then compared to the siderophores dataset obtained through high resolution MS. Spelling and nomenclature differences between our siderophore dataset and antiSMASH database were prior checked and corrected. To infer potential producers of skipped siderophores,

query search was expanded beyond the aerobactin pathway type, namely BGC containing IucA/IucC biosynthetic genes family by targeting other siderophore BGC relevant genes such as transporters.[24] We thus combined secondary metabolism gene families (smCOG) genes annotation from relevant synthesis pathways for these siderophores, namely core biosynthetic genes along specific transporters (e.g. ABC-transporters, MFS, etc.) to mine the antiSMASH database again (Table S2).

3. RESULTS

3.1. Method validation

To evaluate siderophores recovery and enrichment with the SPE-LC platform, seven commercial siderophores standards ranging between 741 Da (ferrichrome, FCH) and 1053 Da (ferrichrome A, FCH-A) were used. Comparison of standards samples in water matrix analyzed with LC, versus when spiked in peat sample, subjected to filtration, and analyzed with SPE-LC-MS, resulted in a global methodological recovery for the set of siderophores considering filtration, SPE enrichment, and potential matrix effects of 74±6%. That was translated into a sample preconcentration factor of 92±8. This preconcentration factor enabled the detection of siderophores in peat matrix in concentrations as low as 40 fmol siderophore per gram of peat.

Optimization and validation of MS identification was carried out for the siderophores standards at the LOD concentration range. Optimized search values of mass tolerance of 3 ppm and intensity tolerance of 30% enabled successful identification of standards through databases mass search. Siderophores identification was observed, however sometimes unsuccessful in the case of FCH-A standard at the LOD concentration range, mostly likely because of lower resolution at higher m/z.[18] The use of list of known siderophores[1] to assist database identification enabled improvement of identification accuracy and success rate and minimizing potential identification mismatches.

Metallophores non-target identification through characteristic isotope pattern of the metal complex was evaluated with the siderophores standards. In all the cases, up to 50 ppt, M-2 (^{54}Fe $[M+H]^+$) and M+1 (^{57}Fe $[M+H]^+$) were detected with mass error lower than 3 ppm for all three isotopologues, M-2, M (^{56}Fe monoisotopic), and M+1 (Fig S4). Below 50 ppt, M+1 was still observed in all cases, but M-2 was only observed for triacetylfusarinine C (TFAC). That is, despite the lower abundance of minor Fe isotopologues (5.8% ^{54}Fe, 2.1% ^{57}Fe) with respect to ^{56}Fe (91.7%), which results in lower S/N ratio and even somewhat higher mass errors as previously stated, it was possible to determine them with sufficient sensitivity and accuracy at such low siderophore concentration levels.

We have herein achieved with the developed 2D-LC-MS approach the detection of siderophores below lowest concentration ranges reported for siderophores in peatlands (~480 pmol/g).[14] It has proved the ability to identify natural isotope patterns of siderophores in peat matrix close to LOD level. Combination with high-resolution MS has resulted in a powerful tool to carry out together the mass-based database identification of known metallophores together with the discovery of novel metal complexes in native non-modified environmental samples.

3.2. Identification of siderophore pool and potential bacteria producers

The analysis of environmental sample with the SPE-LC-MS methodology developed resulted in the identification of 53 siderophores through mass-based database search (Fig 2). Among them, 40 were found solely in their apo form, whereas 13 were also found complexed with iron (ferryl form), though in less abundance than their non-complexed counterpart. Among the identified siderophores, mass-based online databases identification had an efficiency of 83%, missing 9 siderophores found with reference siderophore list. There was one case of controversy, in which two different m/z (599.2099 and 616.2368) were identified by database as the same compound, Heterobactin A. Apparently, despite previous studies identified Heterobactin A to be a species with m/z

599,[26,27] Bosello and coworkers recently reported that this species is presumably the loss of an ammonia group from Heterobactin A, hence the species found at m/z 616 is indeed the actual Heterobactin A.[28] Interestingly, they also reported other Heterobactins (S1 and S2) produced by *Rhodococcus erythropolis*, as well as sulfonated forms of Heterobactin.

Among the 53 siderophores identified in the Bernadouze peat, 16 were recognized as fungal siderophores and 37 corresponded to bacterial metabolites. We focused therein on bacterial siderophores to infer putative producers using both literature search and antiSMASH database mining relying on the composition of the microbial community (Figure 3). Only eleven of the 37 MS-detected prokaryotic siderophores were retrieved from the antiSMASH siderophore database limiting the detection of siderophores other than those sharing aerobactin (hydroxamate type) synthesis pathway.[24] The peat prokaryotic community, as characterised using metabarcoding, comprised 289 ASVs. The phyla *Acidobacteria*, *Proteobacteria* and *Bacteroidota* were predominant (~60% of total ASVs) (Fig 3). The mining of antiSMASH database identified 13 genera as potential siderophore producers in the peat prokaryotic community (Table 1). Six of these genera contained genes similar to BGC involved in the synthesis of six out of the eleven of siderophores both detected in the peat and present in the database: putrebactin / avaroferrin (*Bacillus, Mucilaginibacter, Paraburkholderia, Pseudomonas*), desferroxiamine (*Burkholderia*), desferroxiamine B (*Paraburkholderia*, *Pseudomonas*), desferreoxiamine E (*Cytophaga, Paraburkholderia, Pseudomonas*), bisucaberin B (*Paraburkholderia*), acinetoferrin (*Pseudomonas*) and pyoverdine (*Pseudomonas*). BGC found in the genome of these siderophore producer candidates shared from 8% to 80% of the genes of the MIBiG referenced BGC underlying that BGC of some of these potential siderophore producers may exhibit novelties in their gene composition. No siderophores potentially synthesized by the remaining seven genera (Bradyrhizobium, Collimonas, Coxiella, Lysinibacillus, Methylocystis, Rhodanobacter, Tumebacillus) were detected in the sample.

Mining was then expanded further to the whole antiSMASH database to target additional siderophore BGC relevant genes such as transporters[24] along with specific core biosynthetic genes. Whereas eleven additional siderophores were found, no more taxa were retrieved. Thus, some of the putative producers first identified could also be candidate for the synthesis of cupriachelin and quinolobactin (*Pseudomonas*), enterobactin (*Pseudomonas*) and paenibactin *(Burkholderia, Bacillus)*.

The literature search pointed to microorganisms both known to produce some of the siderophores detected in the peat sample and whose occurrence has been previously documented in peatlands (Table 1). Hence, aerobactin, corrugatin and quinolobactin, have been reported to be produced by different *Pseudomonas* strains (*Pseudomonas sp. strain X40*., *Pseudomonas corrugata* and *Pseudomonas fluorescens ATCC 17400,* respectively).[29–31] Also siderophores vicibactin, vicibactin 7101[32] and rhizobactin 1021,[33] which biosynthesis was documented in rhizobiales species, might also be produced by these microorganisms in the peat, where representatives were identified.

The predominant siderophores found in the Bernadouze peatland sample, in the range of µmol/g, were Serratiochelins (Figure 2c). For these compounds, although all three different forms A, B, and C have been reported to be able to complex iron,[34] just Serratiochelins A was also found in its ferryl form (m/z 483.0727) (Figure 2b). Only apo form of Serratiochelins B was observed (m/z 448.1709). Besides A and B, there is another form of Serratiochelins, Serratiochelins C, which has been detected together with A and B at m/z of 430.1610 (corresponding to loss of water molecule). This m/z is similar to Serratiochelins A apo form (m/z 430.1605), hence targeted MS/MS analysis was performed in order to determine the identity of the compound. In the MS/MS spectra, fragments at m/z 211.11, 237.12 and 294.14, corresponding to apo Serratiochelins A (m/z 430.1605) were observed (Figure 2b).[34] We also observed species at m/z 416.1455 and 444.1195, which could be the product of CH_2 loss and gain, respectively, for

Serratiochelins A (mass difference of 14.0158). Interestingly, sulfonated form of Serratiochelins A was also likely found at m/z 510.1185 (mass difference of 95.9574).

Despite the prevalence of serratiochelins in the Bernadouze peat sample, we did not identify candidate producers in the peat community. Indeed, *Serratia spp*. a genus associated with the keystone Spaghum peat moss peatlands[35,36] was not found in the peat sample. Thus, the presence and high abundance of serratochelins in the Bernadouze's peat might indicate that *Serratia* closely related species thrived as well there. This was also the case for *Shewanella putrefaciens* known to produce putrebactin, avaroferrin and bisucaberinb,[37] *Cupriavidus necator* for cupriachelin [38], *Micrococcus luteus* acyl-desferroxiamine 1,[39] and *Rhodococcus erythropolis for* heterobactins,[27] *Penibacillus elgii B69* for paenibactin[40] and different *Streptomyces* isolates for acyl-desferroxiamine 1, benarthin, desferroxiamine D2, desferroxiamine X1.[1,41–43]

Other siderophores identified in the fmol/g range were synechobactins. Although no ferryl form was identified through isotope pattern matching, a peak observed at m/z 614.2612 presumably corresponds to ferryl form of Synechobactin A (mass difference of 52.9119, Δm of 0.8ppm to $C_{26}H_{46}N_4O_9Fe$),[44] at a concentration range three times lower than the apo form. In the case of Synechobactin B and C, only apo forms were observed. Interestingly, identification of synechobactins siderophores in the sample was unexpectedly not accompanied by the identification of associated siderophore schizokinen.[44] In contrast, other shizokinen-like siderophores reported from terrestrial bacteria like Rhizobactin 1201,[45] or acinetoferrin,[46] were indeed found in Bernadouze peatland. Main known producers of synechobactins belong to freshwater/marine bacterium *Synechoccocus genera.*[47] Interestingly, close related *neosynecoccus* isolates have been reported in continental peat bog as free-living and *Sphagnum* associated.[48] Nevertheless, to date no data indicates that these organisms might also produce synechobactins. Because our sample was collected in the peat and not at the surface

where Sphagnum thrives, it makes sense that we did not recover this genus deeper in the peat community.

SPE-LC-MS analytical platform herein developed resulted in the identification of 53 siderophores both in their apo and ferric forms, demonstrating the possibilities to carry out the inventory of metallophores in native environments. Nonetheless, this approach is constricted to the presence of metallophores in databases, and discovery of novel siderophores shall be evaluated with further developed software tools, e.g. through fragmentation pattern recognition of siderophores families, or creation of artificial isotope patterns through metal complexation. In addition, the inference approach relying on both antiSMASH database mining, and the literature search allowed to evidence putative producers in the peat prokaryotic community. With antiSMASH only, around 30% of the detected bacterial metallophores were associated to a potential known producer, this percentage raised to 52% when highly similar structures (bisucaberins, deferroxiamines, serratochelins, synechobactins, vicibactins) were grouped. Interestingly, these candidates do not belong to the predominant microorganisms in the peat community. Inferences about producers in the environment should therefore be taken with caution for several reasons. First, some siderophores can be synthesized by distantly related microorganisms.[49] For instance, in acidic fen, it has been reported that the strain *Pseudomonas sp. FEN*, can synthesize and use Rhizobactin B,[50] as Rhizobiales. Second, current knowledge on siderophore producers is largely skewed towards cultivated microorganism and overstudied microorganisms.[51] Third, although metabarcoding allows to obtain a good representation of the composition of a community, it does not guarantee an exhaustive representation of this community, likely hiding some of the rarest microorganisms. Fourth, siderophore might be transported by diffusion far from the place where they were synthetized. Finally, as with any inference methods, our antiSMASH mining approach has its own limitations. Therefore, expert

downstream inspection would be required to consider other characteristics such as the size and completeness of the BGCs for more accurate prediction.

3.3. Finding of natural metal complexes

High sensitivity detection of natural isotope pattern of metal complexes achieved with the developed 2D-LC-MS platform, as previously commented, was validated with siderophores standards spiked in peat even at low pM range (Fig S5). In the case of the 13 identified siderophores in their ferryl forms, isotope pattern was identified for aerobactin, corrugatin, enterobactin, fusarinine C, rhizoferrin and serratiochelins A. Missed identification of rest of siderophores does not correlate with estimated abundance, hence improvement in detection seems plausible with enhanced and more powerful dedicated and/or developed software tools.

Yet this identification of metal isotopic patterns along the SPE-LC-MS analysis implies a direct approach for potential *non-target* and *de-novo* identification of metal complexes. That is, metallophores complexed to iron and other multi-isotopic metals as well. To evaluate the presence of metal complexes besides iron ones, Bernadouze peat sample was analyzed with ICP-MS to monitor the profile of metals (Cu, Zn, Mo, Ni, Co, and Fe). Although the obtained metal profiles showed barely any signal besides Fe, low intense peaks were observed for Cu and Mo (Fig 2a, S6). Search for Fe, Mo and Cu complexes isotope patterns with optimized search parameters was carried out, resulting in the finding of 52 Fe(III) and 25 Cu(II) potential metal complexes (Fig 2d, S7). In the case of Fe-complexes, 5 matches resulted also in the finding of mass at 52.91Th lower, in agreement with potential apo form. Despite higher Fe:siderophore stoichimetries have been reported at low and neutral pH conditions, none was observed in the sample.[52,53] Determination of the identity of the detected potential complexes could not be assured. In the case of some compounds, a molecular formula that fits the Mw and isotope pattern observed could be proposed.

De-novo identification of metallophores is limited to the presence of the corresponding metal-complex of each siderophore. In this case, to address the observed limitations in metal complexes identification, promotion of the concentration of iron complexes concentration was evaluated following established procedures of environmental sample incubation with iron.[3,16] Excess iron addition however did not show increase of iron complexation of abundant siderophores with predominant apo form like serratiochelins A, aerobactin or enterobactin. Interestingly, ferryl form increase was observed for rhizoferrin (Fig S8) which, in contrast, has lower complexation constant (log K_{ML} 25.3) than aerobactin (27.6) or enterobactin (49) (Fig S9).[54] Iron complexation requires modifying the native environment of the sample and seems influenced by physicochemical properties of the sample, which could strength the hypothesis that incubation with enriched isotopes is conditioned by matrix nature.[14] This observance would be significant when creating artificial pattern tags in complex peatland-like samples, resulting in the unsuccessful identification and discovery of the siderophores present in it.

The behavior observed in promoted siderophores metal complexation in these preliminary tests, though non-conclusive, points towards furthering the studies on a significant number of complex samples in different environments. It is worth remarking that the proposed methodology can characterize the native sample and provide a reference pool for the better study of metal complexation and exchange processes in any environmental sample.

4. DISCUSSION

This paper reports a novel analytical methodology for the large-scale identification of metallophores in environmental samples by means of the highly sensitive detection of minor isotopologues of the natural isotope pattern of complexed metals, together with high instrumental resolution to identify through the molecular mass metallophores with

error within 3 ppm. Combination of both non-target (though metal isotope pattern) and target (through mass-based database search) identification provides a platform able to provide the characterization of the native environment of an environmental sample extract siderophores pool, without modification of the sample or alteration of such native environment, assuring higher efficiency in the number of siderophores present identified. This assumption is further strengthened by the fact that no characterization, evaluation or mention to this potential incomplete complexation has been addressed in the works that use this kind of approach for siderophores identification. The potential and improvement possibilities of the methodology, particularly in terms of data treatment and intelligent data statistics, may enable a more efficient and faster identification of siderophores without resorting to siderophores list for the correction of missed matches. In this regard, integrative bioinformatic platforms that combine comprehensive information from high-resolution mass spectrometry and enhanced online databases (which would be improved with time) could be a significant step towards a high-throughput platform to characterize metallophores in any environment. In addition, the development of artificial intelligent in computational omics,[70] and the synergy of machine learning with high-throughput data analysis platforms could have a significant impact in multimomics studies, and metallophores discovery in particular.

The study of metallophores and the identification of major contributors to the metallophore pool in complex environments present, to date, many challenges. The companion inference method proposed in this study could be useful for designing targeted molecular analyses to assess the actual contribution of putative producers in

the metallophore pool identified by analytical approaches and reveal as yet unknown siderophore producers. Together with complementary approaches, such as metagenome mining,[51] we can reasonably expect to address the importance of metallophores in structuring complex microbial communities in the near future.

SUPPORTING INFORMATION

The supporting information contains detailed experimental procedures and analysis. Taxonomic-based inference method proposed for fast-screening of potential siderophore producers. Evaluation of mass-based and metal isotope pattern-based identification of ferryl siderophores standards with SPE-LC-MS. List of identified metallophores on Bernadouze peatland. List of metallic complexes found in Bernadouze peatland though isotope pattern match. Analysis of results on studies regarding siderophores complexation with ironmatch. Analysis of results on studies regarding siderophores complexation with iron.

ACKNOWLEDGEMENTS

This project was cofunded by the E2S-UPPA program (Hub-MeSMic project), the LabEx DRIIHM OHM Haut Vicdessos/Haute Vallée des Gaves (METAMIC project), and by the French National Program EC2CO (Ecosphère Continentale et Côtière). We are indebeted to Marnix Medema and Zacchary Reitz (Bioinformatic group, Wageningen University) for helpful discussion and to the Campus France Hubert Curien Partenership (PHC) Van Gogh program (projet n°48064VF) which funded scientific exhanges with M.M. and Z.R.

ORCID

Francisco Calderón Celis: 0000-0003-0331-1595

Iván González Álvarez: 0000-0001-6452-1698

Magdalena Fabjanowicz: 0000-0003-2040-9287

Simon Godin: 0000-0003-3030-8332

Laurent Ouerdane: 0000-0002-2752-3579

Beatrice Lauga: 0000-0001-5997-1176

Ryszard Lobinski: 0000-0003-1908-2029

REFERENCES

(1) Hider, R. C.; Kong, X. Chemistry and Biology of Siderophores. *Nat Prod Rep* **2010**, *27* (5), 637. https://doi.org/10.1039/b906679a.

(2) Mawji, E.; Gledhill, M.; Milton, J. A.; Tarran, G. A.; Ussher, S.; Thompson, A.; Wolff, G. A.; Worsfold, P. J.; Achterberg, E. P. Hydroxamate Siderophores: Occurrence and Importance in the Atlantic Ocean. *Environ Sci Technol* **2008**, *42* (23), 8675–8680. https://doi.org/10.1021/es801884r.

(3) Deicke, M.; Mohr, J. F.; Roy, S.; Herzsprung, P.; Bellenger, J.-P.; Wichard, T. Metallophore Profiling of Nitrogen-Fixing *Frankia* Spp. to Understand Metal Management in the Rhizosphere of Actinorhizal Plants. *Metallomics* **2019**, *11* (4), 810–821. https://doi.org/10.1039/c8mt00344k.

(4) Ortúzar, M.; Trujillo, M. E.; Román-Ponce, B.; Carro, L. Micromonospora Metallophores: A Plant Growth Promotion Trait Useful for Bacterial-Assisted Phytoremediation? *Science of The Total Environment* **2020**, *739*, 139850. https://doi.org/10.1016/j.scitotenv.2020.139850.

(5) Zhang, L.; Dong, H.; Li, R.; Liu, D.; Bian, L.; Chen, Y.; Pan, Z.; Boyanov, M. I.; Kemner, K. M.; Wen, J.; Xia, Q.; Chen, H.; O'Loughlin, E. J.; Wang, G.; Huang, Y. Effect of Siderophore DFOB on U(VI) Adsorption to Clay Mineral and Its Subsequent Reduction by an Iron-Reducing Bacterium. *Environ Sci Technol* **2022**, *56* (17), 12702–12712. https://doi.org/10.1021/acs.est.2c02047.

(6) Zhang, D.; Liu, X.; Guo, D.; Li, G.; Qu, J.; Dong, H. Cr(VI) Reduction by Siderophore Alone and in Combination with Reduced Clay Minerals. *Environ Sci Technol* **2022**, *56* (17), 12315–12324. https://doi.org/10.1021/acs.est.2c04104.

(7) Grobelak, A.; Hiller, J. Bacterial Siderophores Promote Plant Growth: Screening of Catechol and Hydroxamate Siderophores. *Int J Phytoremediation* **2017**, *19* (9), 825–833. https://doi.org/10.1080/15226514.2017.1290581.

(8) Maldonado-Hernández, J.; Román-Ponce, B.; Arroyo-Herrera, I.; Guevara-Luna, J.; Ramos-Garza, J.; Embarcadero-Jiménez, S.; Estrada de los Santos, P.; Wang, E. T.; Vásquez-Murrieta, M. S. Metallophores Production by Bacteria Isolated from Heavy Metal-Contaminated Soil and Sediment at Lerma–Chapala Basin. *Arch Microbiol* **2022**, *204* (3), 180. https://doi.org/10.1007/s00203-022-02780-6.

(9) Roskova, Z.; Skarohlid, R.; McGachy, L. Siderophores: An Alternative Bioremediation Strategy? *Science of The Total Environment* **2022**, *819*, 153144. https://doi.org/10.1016/j.scitotenv.2022.153144.

(10) Tyc, O.; Song, C.; Dickschat, J. S.; Vos, M.; Garbeva, P. The Ecological Role of Volatile and Soluble Secondary Metabolites Produced by Soil Bacteria. *Trends Microbiol* **2017**, *25* (4), 280–292. https://doi.org/10.1016/j.tim.2016.12.002.

(11) Butaitė, E.; Baumgartner, M.; Wyder, S.; Kümmerli, R. Siderophore Cheating and Cheating Resistance Shape Competition for Iron in Soil and Freshwater Pseudomonas Communities. *Nat Commun* **2017**, *8* (1), 414. https://doi.org/10.1038/s41467-017-00509-4.

(12) Kraemer, S. M.; Duckworth, O. W.; Harrington, J. M.; Schenkeveld, W. D. C. Metallophores and Trace Metal Biogeochemistry. *Aquat Geochem* **2015**, *21* (2–4), 159–195. https://doi.org/10.1007/s10498-014-9246-7.

(13) Kraepiel, A. M. L.; Bellenger, J. P.; Wichard, T.; Morel, F. M. M. Multiple Roles of Siderophores in Free-Living Nitrogen-Fixing Bacteria. *BioMetals* **2009**, *22* (4), 573–581. https://doi.org/10.1007/s10534-009-9222-7.

(14) Rai, V.; Fisher, N.; Duckworth, O. W.; Baars, O. Extraction and Detection of Structurally Diverse Siderophores in Soil. *Front Microbiol* **2020**, *11*, 2165. https://doi.org/10.3389/FMICB.2020.581508/BIBTEX.

(15) Singh, A.; Mishra, A. K.; Singh, S. S.; Sarma, H. K.; Shukla, E. Influence of Iron and Chelator on Siderophore Production in *Frankia* Strains Nodulating *Hippophae Salicifolia* D. Don. *J Basic Microbiol* **2008**, *48* (2), 104–111. https://doi.org/10.1002/jobm.200700262.

(16) Deicke, M.; Mohr, J. F.; Bellenger, J.-P.; Wichard, T. Metallophore Mapping in Complex Matrices by Metal Isotope Coded Profiling of Organic Ligands. *Analyst* **2014**, *139* (23), 6096–6099. https://doi.org/10.1039/C4AN01461H.

(17) Rezanezhad, F.; Price, J. S.; Quinton, W. L.; Lennartz, B.; Milojevic, T.; Van Cappellen, P. Structure of Peat Soils and Implications for Water Storage, Flow and Solute Transport: A Review Update for Geochemists. *Chem Geol* **2016**, *429*, 75–84. https://doi.org/10.1016/j.chemgeo.2016.03.010.

(18) Boiteau, R. M.; Fansler, S. J.; Farris, Y.; Shaw, J. B.; Koppenaal, D. W.; Pasa-Tolic, L.; Jansson, J. K. Siderophore Profiling of Co-Habitating Soil Bacteria by Ultra-High Resolution Mass Spectrometry. *Metallomics* **2019**, *11* (1), 166–175. https://doi.org/10.1039/C8MT00252E.

(19) Bolyen, E.; Rideout, J. R.; Dillon, M. R.; Bokulich, N. A.; Abnet, C. C.; Al-Ghalith, G. A.; Alexander, H.; Alm, E. J.; Arumugam, M.; Asnicar, F.; Bai, Y.; Bisanz, J. E.; Bittinger, K.; Brejnrod, A.; Brislawn, C. J.; Brown, C. T.; Callahan, B. J.; Caraballo-Rodríguez, A. M.; Chase, J.; Cope, E. K.; da Silva, R.; Diener, C.; Dorrestein, P. C.; Douglas, G. M.; Durall, D. M.; Duvallet, C.; Edwardson, C. F.; Ernst, M.; Estaki, M.; Fouquier, J.; Gauglitz, J. M.; Gibbons, S. M.; Gibson, D. L.; Gonzalez, A.; Gorlick, K.; Guo, J.; Hillmann, B.; Holmes, S.; Holste, H.; Huttenhower, C.; Huttley, G. A.; Janssen, S.; Jarmusch, A. K.; Jiang, L.; Kaehler, B. D.; Kang, K. bin; Keefe, C. R.; Keim, P.; Kelley, S. T.; Knights, D.; Koester, I.; Kosciolek, T.; Kreps, J.; Langille, M. G. I.; Lee, J.; Ley, R.; Liu, Y.-X.; Loftfield, E.; Lozupone, C.; Maher, M.; Marotz, C.; Martin, B. D.; McDonald, D.; McIver, L. J.; Melnik, A. v.; Metcalf, J. L.; Morgan, S. C.; Morton, J. T.; Naimey, A. T.; Navas-Molina, J. A.; Nothias, L. F.; Orchanian, S. B.; Pearson, T.; Peoples, S. L.; Petras, D.; Preuss, M. L.; Pruesse, E.; Rasmussen, L. B.; Rivers, A.; Robeson, M. S.; Rosenthal, P.; Segata, N.; Shaffer, M.; Shiffer, A.; Sinha, R.; Song, S. J.; Spear, J. R.; Swafford, A. D.; Thompson, L. R.; Torres, P. J.; Trinh, P.; Tripathi, A.; Turnbaugh, P. J.; Ul-Hasan, S.; van der Hooft, J. J. J.; Vargas, F.; Vázquez-Baeza, Y.; Vogtmann, E.; von Hippel, M.; Walters, W.; Wan, Y.; Wang, M.; Warren, J.; Weber, K. C.; Williamson, C. H. D.; Willis, A. D.; Xu, Z. Z.; Zaneveld, J. R.; Zhang, Y.; Zhu, Q.; Knight, R.; Caporaso, J. G. Reproducible, Interactive, Scalable and Extensible Microbiome Data Science Using QIIME 2. *Nat Biotechnol* **2019**, *37* (8), 852–857. https://doi.org/10.1038/s41587-019-0209-9.

(20) Callahan, B. J.; McMurdie, P. J.; Rosen, M. J.; Han, A. W.; Johnson, A. J. A.; Holmes, S. P. DADA2: High-Resolution Sample Inference from Illumina Amplicon Data. *Nat Methods* **2016**, *13* (7), 581–583. https://doi.org/10.1038/nmeth.3869.

(21) Quast, C.; Pruesse, E.; Yilmaz, P.; Gerken, J.; Schweer, T.; Yarza, P.; Peplies, J.; Glöckner, F. O. The SILVA Ribosomal RNA Gene Database Project: Improved Data Processing and Web-Based Tools. *Nucleic Acids Res* **2012**, *41* (D1), D590–D596. https://doi.org/10.1093/nar/gks1219.

(22) Bokulich, N. A.; Kaehler, B. D.; Rideout, J. R.; Dillon, M.; Bolyen, E.; Knight, R.; Huttley, G. A.; Gregory Caporaso, J. Optimizing Taxonomic Classification of Marker-Gene Amplicon Sequences with QIIME 2's Q2-Feature-Classifier Plugin. *Microbiome* **2018**, *6* (1), 90. https://doi.org/10.1186/s40168-018-0470-z.

(23) Blin, K.; Shaw, S.; Kautsar, S. A.; Medema, M. H.; Weber, T. The AntiSMASH Database Version 3: Increased Taxonomic Coverage and New Query Features for Modular Enzymes. *Nucleic Acids Res* **2021**, *49* (D1), D639–D643. https://doi.org/10.1093/nar/gkaa978.

(24) Crits-Christoph, A.; Bhattacharya, N.; Olm, M. R.; Song, Y. S.; Banfield, J. F. Transporter Genes in Biosynthetic Gene Clusters Predict Metabolite Characteristics and Siderophore Activity. *Genome Res* **2021**, *31* (2), 239–250. https://doi.org/10.1101/gr.268169.120.

(25) Wickham, H.; François, R.; Henry, L.; Müller, K.; Vaughan, D. Dplyr: A Grammar of Data Manipulation. *https://dplyr.tidyverse.org, https://github.com/tidyverse/dplyr.* 2023.

(26) Bergeron, R. J.; Singh, S.; Bharti, N. Synthesis of Heterobactins A and B and Nocardia Heterobactin. *Tetrahedron* **2011**, *67* (18), 3163–3169. https://doi.org/10.1016/j.tet.2011.03.003.

(27) Carrano, C. J.; Jordan, M.; Drechsel, H.; Schmid, D. G.; Winkelmann, G. Heterobactins: A New Class of Siderophores from Rhodococcus Erythropolis IGTS8 Containing Both Hydroxamate and Catecholate Donor Groups. *Biometals 2001 14:2* **2001**, *14* (2), 119–125. https://doi.org/10.1023/A:1016633529461.

(28) Bosello, M.; Zeyadi, M.; Kraas, F. I.; Linne, U.; Xie, X.; Marahiel, M. A. Structural Characterization of the Heterobactin Siderophores from *Rhodococcus Erythropolis* PR4 and Elucidation of Their Biosynthetic Machinery. *J Nat Prod* **2013**, *76* (12), 2282–2290. https://doi.org/10.1021/np4006579.

(29) Buyer, J. S.; de Lorenzo, V.; Neilands, J. B. Production of the Siderophore Aerobactin by a Halophilic Pseudomonad. *Appl Environ Microbiol* **1991**, *57* (8), 2246–2250. https://doi.org/10.1128/aem.57.8.2246-2250.1991.

(30) Mossialos, D.; Meyer, J.-M.; Budzikiewicz, H.; Wolff, U.; Koedam, N.; Baysse, C.; Anjaiah, V.; Cornelis, P. Quinolobactin, a New Siderophore of Pseudomonas Fluorescens ATCC 17400, the Production of Which Is Repressed by the Cognate Pyoverdine. *Appl Environ Microbiol* **2000**, *66* (2), 487–492. https://doi.org/10.1128/AEM.66.2.487-492.2000.

(31) Risse, D.; Beiderbeck, H.; Taraz, K.; Budzikiewicz, H.; Gustine, D. Corrugatin, a Lipopeptide Siderophore from Pseudomonas Corrugata. *Zeitschrift für Naturforschung C* **1998**, *53* (5–6), 295–304. https://doi.org/10.1515/znc-1998-5-601.

(32) Dilworth, M. J.; Carson, K. C.; Giles, R. G. F.; Byrne, L. T.; Glenn, A. R. Rhizobium Leguminosarum Bv. Viciae Produces a Novel Cyclic Trihydroxamate Siderophore, Vicibactin. *Microbiology (N Y)* **1998**, *144* (3), 781–791. https://doi.org/10.1099/00221287-144-3-781.

(33) Persmark, M.; Pittman, P.; Buyer, J. S.; Schwyn, B.; Gill, P. R.; Neilands, J. B. Isolation and Structure of Rhizobactin 1021, a Siderophore from the Alfalfa Symbiont Rhizobium Meliloti 1021. *J Am Chem Soc* **1993**, *115* (10), 3950–3956. https://doi.org/10.1021/ja00063a014.

(34) Schneider, Y.; Jenssen, M.; Isaksson, J.; Hansen, K. Ø.; Andersen, J. H.; Hansen, E. H. Bioactivity of Serratiochelin A, a Siderophore Isolated from a Co-Culture of Serratia Sp. and Shewanella Sp. *Microorganisms* **2020**, *8* (7), 1042. https://doi.org/10.3390/microorganisms8071042.

(35) Tian, W.; Wang, H.; Xiang, X.; Wang, R.; Xu, Y. Structural Variations of Bacterial Community Driven by Sphagnum Microhabitat Differentiation in a Subalpine Peatland. *Front Microbiol* **2019**, *10*. https://doi.org/10.3389/fmicb.2019.01661.

(36) Kostka, J. E.; Weston, D. J.; Glass, J. B.; Lilleskov, E. A.; Shaw, A. J.; Turetsky, M. R. The Sphagnum Microbiome: New Insights from an Ancient Plant Lineage. *New Phytologist* **2016**, *211* (1), 57–64. https://doi.org/10.1111/nph.13993.

(37) Soe, C. Z.; Telfer, T. J.; Levina, A.; Lay, P. A.; Codd, R. Simultaneous Biosynthesis of Putrebactin, Avaroferrin and Bisucaberin by Shewanella Putrefaciens and Characterisation of Complexes with Iron(III), Molybdenum(VI) or Chromium(V). *J Inorg Biochem* **2016**, *162*, 207–215. https://doi.org/10.1016/j.jinorgbio.2015.12.008.

(38) Kreutzer, M. F.; Kage, H.; Nett, M. Structure and Biosynthetic Assembly of Cupriachelin, a Photoreactive Siderophore from the Bioplastic Producer Cupriavidus Necator H16. *J Am Chem Soc* **2012**, *134* (11), 5415–5422. https://doi.org/10.1021/ja300620z.

(39) D'Onofrio, A.; Crawford, J. M.; Stewart, E. J.; Witt, K.; Gavrish, E.; Epstein, S.; Clardy, J.; Lewis, K. Siderophores from Neighboring Organisms Promote the Growth of Uncultured Bacteria. *Chem Biol* **2010**, *17* (3), 254–264. https://doi.org/10.1016/j.chembiol.2010.02.010.

(40) Wen, Y.; Wu, X.; Teng, Y.; Qian, C.; Zhan, Z.; Zhao, Y.; Li, O. Identification and Analysis of the Gene Cluster Involved in Biosynthesis of Paenibactin, a Catecholate Siderophore Produced by Paenibacillus Elgii B69. *Environ Microbiol* **2011**, *13* (10), 2726–2737. https://doi.org/10.1111/j.1462-2920.2011.02542.x.

(41) HATSU, M.; NAGANAWA, H.; AOYAGI, T.; TAKEUCHI, T. Benarthin: A New Inhibitor of Pyroglutamyl Peptidase. II. Physico-Chemical Properties and Structure Determination. *J Antibiot (Tokyo)* **1992**, *45* (7), 1084–1087. https://doi.org/10.7164/antibiotics.45.1084.

(42) Traxler, M. F.; Watrous, J. D.; Alexandrov, T.; Dorrestein, P. C.; Kolter, R. Interspecies Interactions Stimulate Diversification of the Streptomyces Coelicolor Secreted Metabolome. *mBio* **2013**, *4* (4). https://doi.org/10.1128/mBio.00459-13.

(43) Cooper, R. E.; Eusterhues, K.; Wegner, C.-E.; Totsche, K. U.; Küsel, K. Ferrihydrite-Associated Organic Matter (OM) Stimulates Reduction by ≪I≫Shewanella Oneidensis≪/I≫ MR-1 and a Complex Microbial Consortia. *Biogeosciences* **2017**, *14* (22), 5171–5188. https://doi.org/10.5194/bg-14-5171-2017.

(44) Ito, Y.; Butler, A. Structure of Synechobactins, New Siderophores of the Marine Cyanobacterium *Synechococcus* Sp. PCC 7002. *Limnol Oceanogr* **2005**, *50* (6), 1918–1923. https://doi.org/10.4319/lo.2005.50.6.1918.

(45) Persmark, M.; Pittman, P.; Buyer, J. S.; Schwyn, B.; Gill, P. R.; Neilands, J. B. Isolation and Structure of Rhizobactin 1021, a Siderophore from the Alfalfa Symbiont Rhizobium Meliloti 1021. *J Am Chem Soc* **1993**, *115* (10), 3950–3956. https://doi.org/10.1021/ja00063a014.

(46) Okujo, N.; Sakakibara, Y.; Yoshida, T.; Yamamoto, S. Structure of Acinetoferrin, a New Citrate-Based Dihydroxamate Siderophore FromAcinetobacter Haemolyticus. *Biometals* **1994**, *7* (2). https://doi.org/10.1007/BF00140488.

(47) Leão, P. N.; Engene, N.; Antunes, A.; Gerwick, W. H.; Vasconcelos, V. The Chemical Ecology of Cyanobacteria. *Nat Prod Rep* **2012**, *29* (3), 372. https://doi.org/10.1039/c2np00075j.

(48) DVOŘÁK, P.; HINDÁK, F.; HAŠLER, P.; HINDÁKOVÁ, A.; POULÍČKOVÁ, A. Morphological and Molecular Studies of Neosynechococcus Sphagnicola, Gen. et Sp. Nov. (Cyanobacteria, Synechococcales). *Phytotaxa* **2014**, *170* (1), 024. https://doi.org/10.11646/phytotaxa.170.1.3.

(49) Koppisch, A. T.; Browder, C. C.; Moe, A. L.; Shelley, J. T.; Kinkel, B. A.; Hersman, L. E.; Iyer, S.; Ruggiero, C. E. Petrobactin Is the Primary Siderophore Synthesized by Bacillus Anthracis Str. Sterne under Conditions of Iron Starvation. *BioMetals* **2005**, *18* (6), 577–585. https://doi.org/10.1007/s10534-005-1782-6.

(50) Kügler, S.; Cooper, R. E.; Boessneck, J.; Küsel, K.; Wichard, T. Rhizobactin B Is the Preferred Siderophore by a Novel Pseudomonas Isolate to Obtain Iron from Dissolved Organic Matter in Peatlands. *BioMetals* **2020**, *33* (6), 415–433. https://doi.org/10.1007/s10534-020-00258-w.

(51) Reitz, Z. L.; Medema, M. H. Genome Mining Strategies for Metallophore Discovery. *Curr Opin Biotechnol* **2022**, *77*, 102757. https://doi.org/10.1016/j.copbio.2022.102757.

(52) Codd, R.; Soe, C. Z.; Pakchung, A. A. H.; Sresutharsan, A.; Brown, C. J. M.; Tieu, W. The Chemical Biology and Coordination Chemistry of Putrebactin, Avaroferrin, Bisucaberin, and Alcaligin. *JBIC Journal of Biological Inorganic Chemistry* **2018**, *23* (7), 969–982. https://doi.org/10.1007/s00775-018-1585-1.

(53) Ledyard, K. M.; Butler, A. Structure of Putrebactin, a New Dihydroxamate Siderophore Produced by Shewanella Putrefaciens. *JBIC Journal of Biological Inorganic Chemistry* **1997**, *2* (1), 93–97. https://doi.org/10.1007/s007750050110.

(54) Zhang, G.; Amin, S. A.; Küpper, F. C.; Holt, P. D.; Carrano, C. J.; Butler, A. Ferric Stability Constants of Representative Marine Siderophores: Marinobactins, Aquachelins, and Petrobactin. *Inorg Chem* **2009**, *48* (23), 11466–11473. https://doi.org/10.1021/ic901739m.

(55) Nwugo, C. C.; Gaddy, J. A.; Zimbler, D. L.; Actis, L. A. Deciphering the Iron Response in Acinetobacter Baumannii: A Proteomics Approach. *J Proteomics* **2011**, *74* (1), 44–58. https://doi.org/10.1016/j.jprot.2010.07.010.

(56) Cleto, S.; Haslinger, K.; Prather, K. L. J.; Lu, T. K. Natural Combinatorial Genetics and Prolific Polyamine Production Enable Siderophore Diversification in Serratia Plymuthica. *BMC Biol* **2021**, *19* (1), 46. https://doi.org/10.1186/s12915-021-00971-z.

(57) PAGE, W. J.; TIGERSTROM, M. V. Aminochelin, a Catecholamine Siderophore Produced by Azotobacter Vinelandii. *Microbiology (N Y)* **1988**, *134* (2), 453–460. https://doi.org/10.1099/00221287-134-2-453.

(58) Martinez, J. S.; Zhang, G. P.; Holt, P. D.; Jung, H.-T.; Carrano, C. J.; Haygood, M. G.; Butler, A. Self-Assembling Amphiphilic Siderophores from Marine Bacteria. *Science (1979)* **2000**, *287* (5456), 1245–1247. https://doi.org/10.1126/science.287.5456.1245.

(59) Fujita, M.; Nakano, K.; Sakai, R. Bisucaberin B, a Linear Hydroxamate Class Siderophore from the Marine Bacterium Tenacibaculum Mesophilum. *Molecules* **2013**, *18* (4), 3917–3926. https://doi.org/10.3390/molecules18043917.

(60) Challis, G. L.; Ravel, J. Coelichelin, a New Peptide Siderophore Encoded by the *Streptomyces Coelicolor* Genome: Structure Prediction from the Sequence of Its Non-Ribosomal Peptide Synthetase. *FEMS Microbiol Lett* **2000**, *187* (2), 111–114. https://doi.org/10.1111/j.1574-6968.2000.tb09145.x.

(61) Keller-Schierlein, W.; Roncari, G. Stoffwechselprodukte von Mikroorganismen 46. Mitteilung Die Konstitution Des Lankamycins. *Helv Chim Acta* **1964**, *47* (1), 78–103. https://doi.org/10.1002/hlca.19640470111.

(62) Ejje, N.; Soe, C. Z.; Gu, J.; Codd, R. The Variable Hydroxamic Acid Siderophore Metabolome of the Marine Actinomycete Salinispora Tropica CNB-440. *Metallomics* **2013**, *5* (11), 1519. https://doi.org/10.1039/c3mt00230f.

(63) Chiani, M.; Akbarzadeh, A.; Farhangi, A.; Mazinani, M.; Saffari, Z.; Emadzadeh, K.; Mehrabi, M. R. Optimization of Culture Medium to Increase the Production of Desferrioxamine B (Desferal) in Streptomyces Pilosus. *Pakistan Journal of Biological Sciences* **2010**, *13* (11), 546–550. https://doi.org/10.3923/pjbs.2010.546.550.

(64) Smits, T. H. M.; Duffy, B. Genomics of Iron Acquisition in the Plant Pathogen Erwinia Amylovora: Insights in the Biosynthetic Pathway of the Siderophore Desferrioxamine E. *Arch Microbiol* **2011**, *193* (10), 693–699. https://doi.org/10.1007/s00203-011-0739-0.

(65) Essén, S. A.; Johnsson, A.; Bylund, D.; Pedersen, K.; Lundström, U. S. Siderophore Production by *Pseudomonas Stutzeri* under Aerobic and Anaerobic Conditions. *Appl Environ Microbiol* **2007**, *73* (18), 5857–5864. https://doi.org/10.1128/AEM.00072-07.

(66) Adapa, S.; Hubtr, P.; Keller-Schierlein, W. Stoffwechselprodukte von Mikroorganismen. 216. Mitteilung. Isolierung, Strukturaufklärung Und Synthese von Ferrioxamin H. *Helv Chim Acta* **1982**, *65* (6), 1818–1824. https://doi.org/10.1002/hlca.19820650617.

(67) Feistner, G. J.; Stahl, D. C.; Gabrik, A. H. Proferrioxamine Siderophores OfErwinia Amylovora. A Capillary Liquid Chromatographic/Electrospray Tandem Mass

Spectrometric Study. *Organic Mass Spectrometry* **1993**, *28* (3), 163–175. https://doi.org/10.1002/oms.1210280307.

(68) Robbel, L.; Knappe, T. A.; Linne, U.; Xie, X.; Marahiel, M. A. Erythrochelin - a Hydroxamate-Type Siderophore Predicted from the Genome of Saccharopolyspora Erythraea. *FEBS Journal* **2010**, *277* (3), 663–676. https://doi.org/10.1111/j.1742-4658.2009.07512.x.

(69) Böttcher, T.; Clardy, J. A Chimeric Siderophore Halts Swarming *Vibrio*. *Angewandte Chemie International Edition* **2014**, *53* (13), 3510–3513. https://doi.org/10.1002/anie.201310729.

(70) Mullowney, M. W.; Duncan, K. R.; Elsayed, S. S.; Garg, N.; van der Hooft, J. J. J.; Martin, N. I.; Meijer, D.; Terlouw, B. R.; Biermann, F.; Blin, K.; Durairaj, J.; Gorostiola González, M.; Helfrich, E. J. N.; Huber, F.; Leopold-Messer, S.; Rajan, K.; de Rond, T.; van Santen, J. A.; Sorokina, M.; Balunas, M. J.; Beniddir, M. A.; van Bergeijk, D. A.; Carroll, L. M.; Clark, C. M.; Clevert, D.-A.; Dejong, C. A.; Du, C.; Ferrinho, S.; Grisoni, F.; Hofstetter, A.; Jespers, W.; Kalinina, O. V.; Kautsar, S. A.; Kim, H.; Leao, T. F.; Masschelein, J.; Rees, E. R.; Reher, R.; Reker, D.; Schwaller, P.; Segler, M.; Skinnider, M. A.; Walker, A. S.; Willighagen, E. L.; Zdrazil, B.; Ziemert, N.; Goss, R. J. M.; Guyomard, P.; Volkamer, A.; Gerwick, W. H.; Kim, H. U.; Müller, R.; van Wezel, G. P.; van Westen, G. J. P.; Hirsch, A. K. H.; Linington, R. G.; Robinson, S. L.; Medema, M. H. Artificial Intelligence for Natural Product Drug Discovery. Nat Rev Drug Discov 2023, 1–22. https://doi.org/10.1038/s41573-023-00774-7.

FIGURES

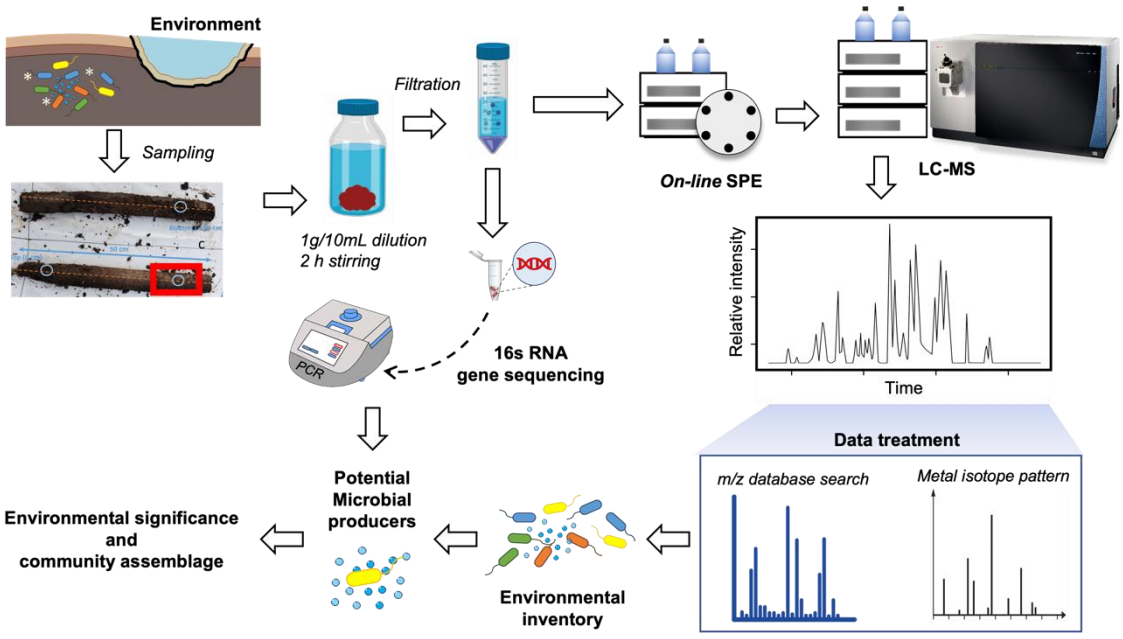

Figure 1. Scheme representation of the methodological approach for the identification of metallophores using on-line SPE-LC-MS and their microbial producers by gene sequencing and antiSMASH database search.

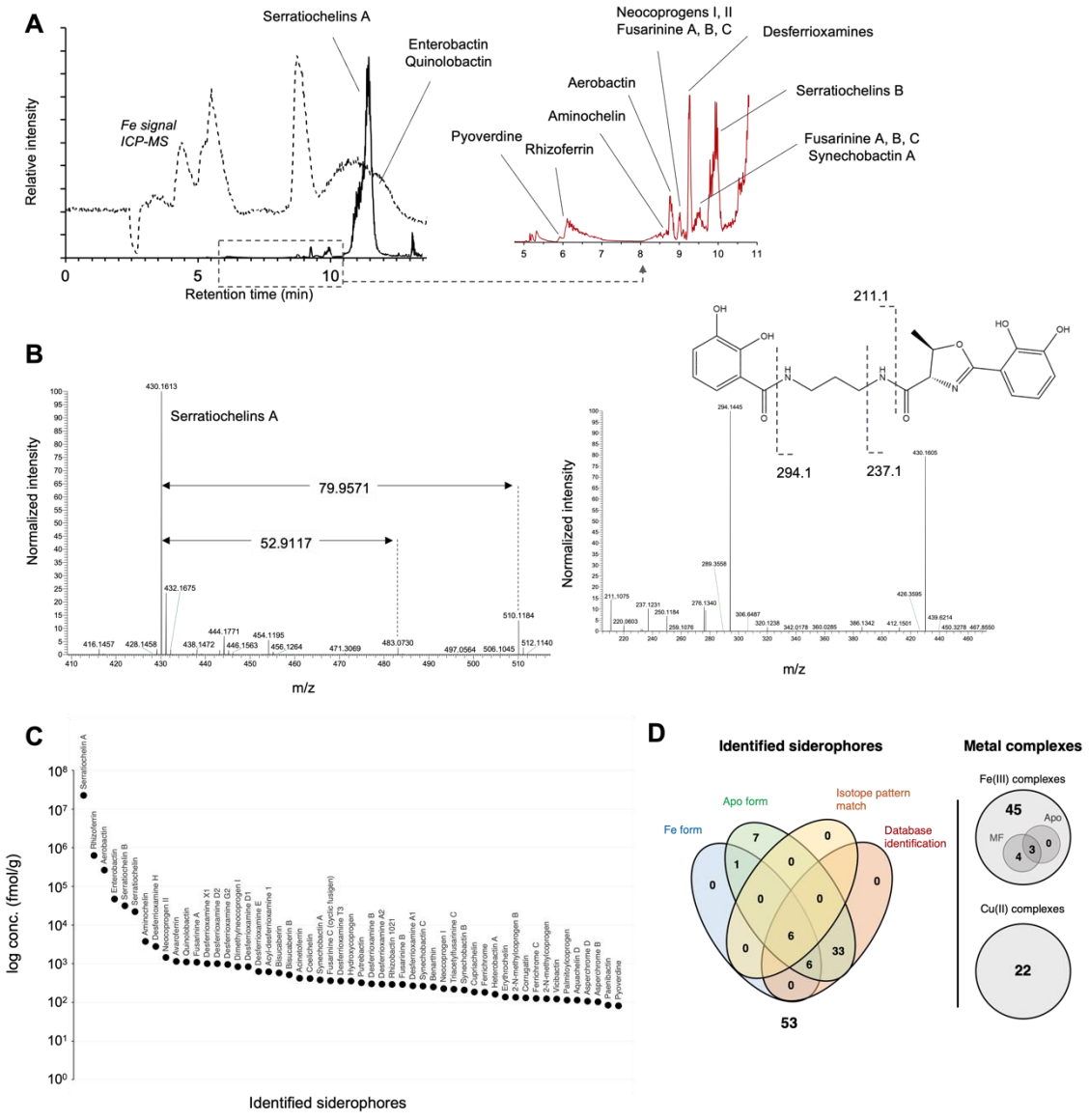

Figure 2. (A) Analysis of Bernadouze peatland water extract with SPE-LC-MS, overlapped with iron signal obtained with SPE-LC-ICP-MS analysis, and remarking the elution of major siderophores identified. (B) MS spectra of Serratiochelins A, in which two species with mass differences of 52.9117 and 79.9571, correlated to ferryl and sulfonate forms, respectively, were observed. On the right, MS/MS spectra of Serratiochelins A, and its structure with the fragmentation observed in the spectra marked with dotted line. (C) Concentration levels of identified siderophores in Bernadouze peatland. Y axis shows log of concentration in fmol siderophore per g of soil. (D) Venn diagrams representing, on the left, the number of siderophores identified in their apo and ferryl form using mass-based databases search (for both apo and ferryl

forms), and metal complex characteristic isotope pattern for ferryl siderophores. On the right, number of non-identified compounds found through isotopic pattern matches corresponding to Fe(III) and Cu(II) complexes, representing as well those for which apo form was found, as well as for those which it was possible to propose molecular formula (MF) matching the observed pattern.

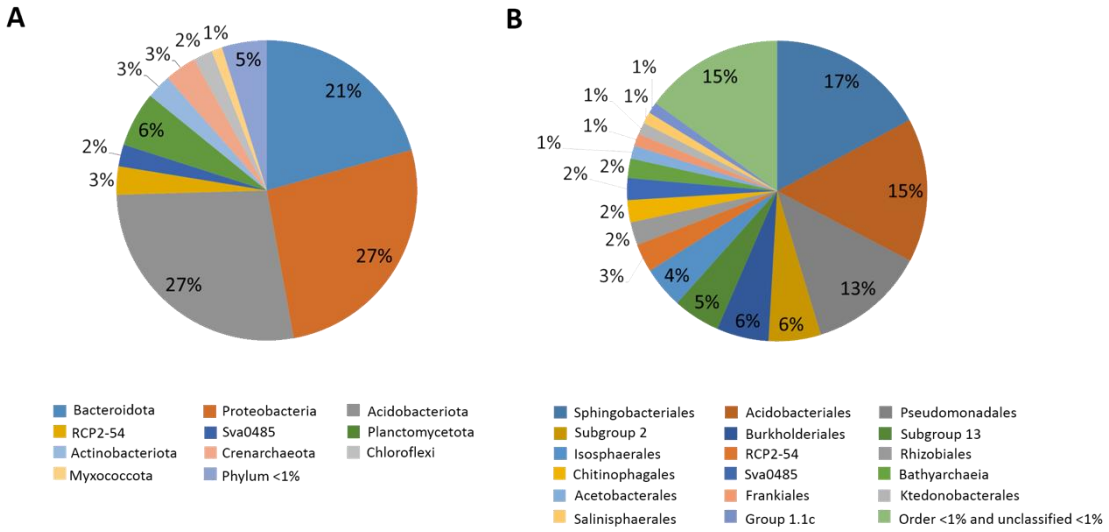

Figure 3. Composition of the peat procaryotic community. Taxonomic profile was revealed by high throughput sequencing targeting 16Sr RNA gene and expressed as relative abundance at the phylum level (A) and order level (B).

TABLES

Table 1. Putative siderophore producers as inferred after antiSMASH mining and bacteria known to produce the siderophore detected in the peat according to literature search. In the first case, for each candidate genus detected in the peat community, BGC percent of similarity (completeness) to the MIBiG reference BGC along its accession number and the organism's name are given. For relevant genes of BGC, according to antiSMASH database nomenclature, core biosynthetic genes are indicated with (a), transporter-related genes with (b), and additional biosynthetic genes with (c). Asterisk (*) indicates bacteria occurring in peatlands or peat related samples along with related references.

Siderophore	antiSMASH inference				Producers according to literature
	Genus detected in Bernadouze peat	% genes similarity (completeness)	MiBIG reference (genus level)	BGC accession #	
Acinetoferrin	*Pseudomonas*[(a)(b)(c)]	20-60%	*Acinetobacter*	BGC0000295	*Acinetobacter*[55]
Acyl-desferrioxamine 1	*Pseudomonas*[(a)(c)]	66%	*Streptomyces*	*BGC0000940*	*Micrococcus**[39]; *Streptomyces**[42]
Aerobactin	/	/	*Grimontia; Xenorhabdus*; *Pantoea*; *Vibrio*	BGC0000939; BGC0001498; BGC0001499; BGC0002682	*Pseudomonas** [29]; *Serratia** [56]; *Shewanella**[37]
Aminochelin	/	/	*Azotobacter*	BGC0002528; BGC0002529	*Azotobacter*[57]
Aquachelin D	/	/		/	*Halomonas*[58]
Benarthin	/	/	*Planobispora*	BGC0002688	*Streptomyces**[41]
Bisucaberin	/	/		/	*Shewanella**[37]
Bisucaberin B	*Paraburkholderia*[(a)(c)]	66%	*Tenacibaculum*	BGC0001531	*Tenacibaculum*[59]
Coelichelin	*Pseudomonas*[(a)(b)(c)]	18%	*Streptomyces*	BGC0000325	*Streptomyces*[60]
Corrugatin	*Pseudomonas*[(a)(b)(c)]	100%	*Pseudomonas*	BGC0002422	*Pseudomonas**[31]
Cupriachelin	*Pseudomonas*[(b)(c)]	11-35%	*Cupriavidus*	BGC0000330	*Cupriavidus**[38]
Desferrioxamine A1	/	/	/	/	*Nocardia, Streptomyces*[61] ; *Salinispora*[62]
Desferrioxamine A2	/	/	/	/	*Nocardia, Streptomyces*[61]
Desferrioxamine B	*Burkholderia*[(a)(c)]; *Paraburkholderia*[(a)(c)]; *Pseudomonas*[(a)(c)]	50%; 60%; 66-80%	*Streptomyces*; *Kribbella*	BGC0000940; BGC0000941; BGC0001453; BGC0002305; BGC0002692	*Streptomyces*[63]
Desferrioxamine D1	/	/	*Kribbella*	BGC0002692	*Nocardia, Streptomyces*[61]
Desferrioxamine D2	/	/	/		*Streptomyces*[1]
Desferrioxamine E	*Cytophaga*[(1,3)]; *Paraburkholderia*[(1,3)]; *Pseudomonas*[(1,3)]	50%; 50%; 66-100%	*Streptomyces*; *Pantonea*	BGC0000940; BGC0001478; BGC0001572	*Erwinia*[64] *Pseudomonas*[65], *Streptomyces*[1]
Desferrioxamine H	/	/	/	/	*Steptomyces** [66]
Desferrioxamine T3	/	/	/	/	*Erwinia* [67]
Desferrioxamine X1	/	/	/	/	*Streptomyces** [1]
Enterobactin	*Pseudomonas*[(1,2,3)]	64%	*Pseudomonas*; *Escherichia*; *Rothia*	BGC0000343; BGC0002476; BGC0002685	*Serratia**[56]
Erythrochelin	/	/	*Saccharopolyspora*	BGC0000349	*Saccharopolyspora*[68]
Heterobactin A	/	/	*Rhodococcus*	BGC0000371	*Rhodococcus*[27]
Paenibactin	*Burkholderia*[(a)(c)]; *Bacillus*[(a)(c)]	66%; 66%	*Paenibacillus*	BGC0000401	*Paenibacillus**[40]
Putrebactin / avaroferrin	*Bacillus*[(2,3)]; *Mucilaginibacter*[(a)(c)]; *Paraburkholderia*[(a)(c)]; *Pseudomonas*[(a)(c)]	20%; 20%; 30%; 20-40%	*Xenorhabdus*	BGC0001870	*Shewanella** [53,69]
Pyoverdin	*Bradyrhizobium*[(a)(b)(c)]; *Pseudomonas*[(a)(b)(c)]; *Sphingomonas*[(a)(b)(c)]	7%; 1-33%; 25%	*Pseudomonas*	BGC0000413; BGC0002571; BGC0002693	*Pseudomonas**[30]
Quinolobactin	*Pseudomonas*[(a)(b)(c)]	80%	*Pseudomonas*	BGC0000925	*Pseudomonas**[30]
Rhizobactin 1021	/	/	*Francisella*	BGC0002681	*Rhizobium**[45]
Serratiochelin	/	/	*Serratia*	BGC0002496	*Serratia**[56]
Serratiochelin A	/	/	*Serratia*	BGC0002496	*Serratia**[56]
Serratiochelin B	/	/	*Serratia*	BGC0002496	*Serratia**[56]
Synechobactin A	/	/	*Synechococcus*	BGC0002470	*Synechococcus*[47]
Synechobactin B	/	/	*Synechococcus*	BGC0002470	*Synechococcus*[47]
Synechobactin C	/	/	*Synechococcus*	BGC0002470	*Synechococcus*[47]
Vicibactin	*Methylocapsa*[(a)(b)(c)]	55%	*Rhizobium*	BGC0000457	*Rhizobium**[32]
Vicibactin 7101	*Methylocapsa*[(a)(b)(c)]	55%	*Rhizobium*	BGC0000457	*Rhizobium**[32]

1

SUPPORTING INFORMATION

Unveiling the Pool of Metallophores in Native Environments and Correlation with Their Potential Producers

Francisco Calderón Celis[1]*, Ivan González-Álvarez[1], Magdalena Fabjanowicz[2], Simon Godin[1], Laurent Ouerdane[1], Béatrice Lauga[1], Ryszard Łobiński[1,3]

[1]*E2S UPPA, CNRS, IPREM, Université de Pau et des Pays de l'Adour, 64000 Pau, France.*

[2]*Faculty of Chemistry, Department of Analytical Chemistry, Gdańsk University of Technology, 80-233 Gdańsk, Poland.*

[3]*Chair of Analytical Chemistry, Warsaw University of Technology, 00-664 Warsaw, Poland.*

*Correspondence: calderonfrancisco@uniovi.es (F.C.C)

Abstract:

The supporting information contains detailed experimental procedures and analysis. Taxonomic-based inference method proposed for fast-screening of potential siderophore producers. Evaluation of mass-based and metal isotope pattern-based identification of ferryl siderophores standards with SPE-LC-MS. List of identified metallophores on Bernadouze peatland. List of metallic complexes found in Bernadouze peatland though isotope pattern match. Analysis of results on studies regarding siderophores complexation with iron.

Experimental procedure:

Chemicals and materials

Formic acid LiChropur for LC-MS was from Merck KGaA (Germany). Acetonitrile and methanol LC-MS Chromasolv (>99.9%) was from Honeywell (Germany). Ammonium formate, purity for mass spectrometry, ≥99%, was from Sigma-Aldrich (Steinheim). Ferric siderophores standards (ferrichrome, ferricrocin, ferrichrysin, coprogen, ferrirhodin, triacetylfusarinine C, ferrichrome A) were purchased from EMC microcollections (Germany).

On-line solid phase extraction with reversed-phase chromatography

Reversed-phase(RP)-liquid chromatography (LC) was carried out at 40ºC using a flow rate of 0.3 mL/min. The mobile phase consisted of 5 mM ammonium formate (Sigma) in water and 0.1% formic acid (v/v) (A) and acetonitrile/methanol (90/10) and 0.1% formic acid (v/v) (B). Samples were injected using a second Dionex HPLC system (Thermo) for on-line solid phase extraction (SPE) (Figure S1). The volume of sample injected was 2.5 mL and was retained in an Oasis HLB Direct Connect HP 20µm, 2.1x300mm On-Line Extraction Column, Waters (Ireland) using a loading phase with the same composition as mobile phase A. Sample injection occurred during chromatographic isocratic step at 2% phase B during 5 min, which was followed by a gradient from 2 to 50% phase B in 2 min, held in isocratic for 1 min, and followed by an increased to 98% phase B in 2 min.

ESI-MS detection of siderophores

Analytes were ionized by heated electrospray ionization operating in the positive ionization mode with the following settings when coupled to SPE-(RP)LC: capillary voltage, 3500 V; Sheath Gas, 50; Aux Gas 10; Sweep Gas 1; Ion Transfer Tube Temp, 350ºC; Vaporizer Temp, 350ºC. Data acquisition settings were: full MS scan; resolution, 500 000; m/z scan range 150-2000; RF Lens, 50%; Normalized automatic gain control target, 25%. MS/MS data were acquired using collision induced dissociation (CID) data-

dependent acquisition method using the following settings: m/z isolation window, 0.5; resolution, 50,000; m/z scan range, 205-2000; CID Collision Energy, 25%; CID Activation Time, 10ms; Activation Q, 0.25; Normalized automatic gain control target, 20%.

Raw LC-MS data was analyzed with Thermo Compound Discoverer 3.1 software. Search parameters were optimized using a solution of siderophores standards at low concentration level (10 and 50 ng/g). Optimal parameters provided successful detection identification of siderophores standards. That is, the lowest mass error and with enough sensitivity to differentiate the signal from the noise background. Analysis workflow consisted of: (i) substract of blank compounds, intensity threshold tolerance sample/blank: 3; (ii) compound identification with local off-line mass list, mass tolerance 3 ppm; (iii) compound mass-based identification with on-line ChemSpider databases search, mass tolerance 3ppm; (iv) location of elemental isotope pattern matches (Fe, Cu, Mo), mass tolerance 3ppm, intensity tolerance 30%.

ICP-MS analysis

SPE-(RP)LC-ICP-MS analyses were carried out using Agilent 7700 ICP-MS instrument (Japan), with organic kit, 1.0 mm i.d. torch, platinum cones and s-lens. Chromatographic conditions were identical to the ones used with ESI-MS detection. Instrumental parameters are summarized in Table S1.

Methodological recovery

To evaluate methodological sample recovery, SPE column performance for siderophores analysis was first compared to LC column. Ferryl siderophores standards were injected independently and at the same concentration in both columns, SPE and LC, for LC analysis. Peak areas comparison resulted in SPE peak areas to be 105 ± 4% of LC peak areas, that is, siderophores are properly retained in the SPE column during the loading phase and eluted during the elution phase. There are no unspecific interactions of siderophores with SPE column even in the environmental matrix, nor are

washed out in the SPE loading stage. On the other hand, when comparing performance of the SPE-LC system to LC, area ratio SPE-LC/LC was observed to be 89 ± 7%, implying virtually quantitative recovery of the siderophores from the chromatographic system. Finally, siderophores signal was compared when spiked in water and analyzed with UPLC, versus when spiked in the sample, subjected to filtration, and analyzed with SPE-UPLC-MS. The global methodological recovery for the set of siderophores considering filtration, SPE enrichment, and potential matrix effects during the analysis, resulted in an average recovery of 74 ± 6%.

Considering the maximum sample volume that can be injected in regular chromatography (20 µL), and the volume of sample injected during the on-line SPE (2.5 mL), and considering the calculated recovery, we could determine that the system results in sample preconcentration factor of 92 ± 8. It is worth remarking that, in addition to sample preconcentration, use of on-line SPE results in a faster, more direct, and simpler procedure than off-line SPE, besides resulting in a cleaner sample introduced in the mass spectrometer, because salts, small contaminants and buffers are washed away during the sample loading in the SPE column.

Evaluation of limit of detection and limit of quantification

Sensitivity of the methodology was evaluated using siderophores standards spiked in the environmental sample at different concentrations ranging from 10 to 1000 ng/L matrix, filtered, and analyzed with SPE-UPLC-MS. Methodological detection limits were calculated from the calibration curve as 3.3σ/s, being σ the standard deviation of the intercept (y) and the slope (s). LOQ was calculated as 10σ/s. LOD obtained for the six ferryl siderophores standards spiked in the peat sample matrix was ranged 5-20 pM, and LOQ was ranged 10-50 pM.

Table S1. ICP-MS acquisition parameters for Agilent 7700 (SEC-ICP-MS) and Agilent 7500 (RP-ICP-MS).

Parameter	Value
Carrier gas (L/min)	0.46
Make-up gas (L/min)	0.1
Dilution gas (L/min)	0.0
Optional gas, O_2 (%)	5
Cell gas, He (mL/min)	4
Sample depth (mm)	8.0
Extract 1 (V)	3
Extract 2 (V)	-140
Omega bias (V)	-40 (S)
Omega lens (V)	9 (S)
Discrimination energy (mV)	4
Integration time (s)	0.1

Table S2. List of siderophores identified in Bernadouze Peatland, including the m/z of the apo form, the m/z of the ferryl form in those cases in which it was identified, the molecular formula, and the elution time.

Identity	$[M+H]^+$ *m/z*	$[M-2H+Fe]^+$ m/z	Molecular formula	Elution time (min)
2-N-methylcoprogen	783.4129		$C_{36}H_{58}N_6O_{13}$	8.7
2-N-methylcoprogen B	741.4036		$C_{34}H_{56}N_6O_{12}$	9.8
Acinetoferrin	585.3481		$C_{28}H_{48}N_4O_9$	10.4
Acyl-desferrioxamine 1	637.3926		$C_{31}H_{52}N_6O_8$	9.3
Aerobactin	565.2346	618.1467	$C_{22}H_{36}N_4O_{13}$	8.9
Aminochelin	225.1237		$C_{11}H_{16}N_2O_3$	8.6
Aquachelin D	1093.5653	1146.4723	$C_{46}H_{80}N_{10}O_{20}$	4.3
Asperchrome B	888.4335		$C_{37}H_{61}N_9O_{16}$	8.9
Asperchrome D	818.3887		$C_{33}H_{55}N_9O_{15}$	8.9
Avaroferrin	387.2242		$C_{17}H_{30}N_4O_6$	9.0
Benarthin	412.1816		$C_{17}H_{25}N_5O_7$	8.6
Bisucaberin	401.2399		$C_{18}H_{32}N_4O_6$	9.0
Bisucaberin B	419.2506		$C_{18}H_{34}N_4O_7$	9.3
Coelichelin	566.2772		$C_{21}H_{39}N_7O_{11}$	9.0
Corrugatin	998.4553	1051.3668	$C_{40}H_{63}N_{13}O_{17}$	9.21
Cupriachelin	808.3954		$C_{33}H_{57}N_7O_{16}$	8.8
Desferrioxamine A1	547.3451		$C_{24}H_{46}N_6O_8$	8.6
Desferrioxamine A2	533.3285		$C_{23}H_{44}N_6O_8$	8.4
Desferrioxamine B	561.3610	614.2723	$C_{25}H_{48}N_6O_8$	8.5
Desferrioxamine D1	603.3733		$C_{27}H_{50}N_6O_9$	8.8
Desferrioxamine D2	587.3402		$C_{26}H_{46}N_6O_9$	9.2
Desferrioxamine E	601.3577	654.2694	$C_{27}H_{48}N_6O_9$	9.1
Desferrioxamine G2	605.3522		$C_{26}H_{48}N_6O_{10}$	8.8
Desferrioxamine H	461.2606		$C_{20}H_{36}N_4O_8$	9.3
Desferrioxamine T3	773.4411		$C_{34}H_{60}N_8O_{12}$	9.2
Desferrioxamine X1	573.3249	626.2359	$C_{25}H_{44}N_6O_9$	8.9
Dimethylneocoprogen I	685.3776	738.2897	$C_{31}H_{52}N_6O_{11}$	9.0
Enterobactin	670.1518	723.0626	$C_{30}H_{27}N_3O_{15}$	11.7
Erythrochelin	604.2941		$C_{24}H_{41}N_7O_{11}$	6.4
Ferrichrome	688.3265		$C_{27}H_{45}N_9O_{12}$	8.7
Ferrichrome C	702.3391	755.2522	$C_{28}H_{47}N_9O_{12}$	9.0
Fusarinine A	503.2694		$C_{22}H_{38}N_4O_9$	9.1
Fusarinine B	745.3993		$C_{33}H_{56}N_6O_{13}$	9.0
Fusarinine C/Coprogen B/Cyclic Fusigen	727.3881	780.2993	$C_{33}H_{54}N_6O_{12}$	9.0
Heterobactin A	616.2369		$C_{27}H_{33}N_7O_{10}$	8.4
Hydroxycoprogen	785.3935		$C_{35}H_{56}N_6O_{14}$	9
Neocoprogen I	699.3567		$C_{31}H_{50}N_6O_{12}$	9.0
Neocoprogen II	629.3161		$C_{27}H_{44}N_6O_{11}$	9.0
Paenibactin	925.3117	978.2235	$C_{42}H_{48}N_6O_{18}$	11.4
Palmitoylcoprogen	965.6198		$C_{49}H_{84}N_6O_{13}$	4.3
Putrebactin	373.2085		$C_{16}H_{28}N_4O_6$	8.6

Table S2. List of siderophores identified in Bernadouze Peatland (cont).

Identity	$[M+H]^+$ *m/z*	$[M-2H+Fe]^+$ m/z	Molecular formula	Elution time (min)
Pyoverdine	559.7287		$C_{45}H_{63}N_{15}O_{19}$	5.8
Quinolobactin	220.0606		$C_{11}H_9N_1O_4$	11.5
Rhizobactin 1021	531.3038		$C_{24}H_{42}N_4O_9$	8.8
Rhizoferrin	437.1402	490.0518	$C_{16}H_{24}N_2O_{12}$	6.1
Serratiochelin	416.1455		$C_{20}H_{21}N_3O_7$	11.5
Serratiochelin A	430.1605	483.0726	$C_{21}H_{23}N_3O_7$	11.5
Serratiochelin B	448.1724		$C_{21}H_{25}N_3O_8$	10.2
Synechobactin A	561.3493		$C_{26}H_{48}N_4O_9$	9.6
Synechobactin B	533.3172		$C_{24}H_{44}N_4O_9$	9.3
Synechobactin C	505.2875		$C_{22}H_{40}N_4O_9$	8.8
Triacetylfusarinine C	853.4205		$C_{39}H_{60}N_6O_{15}$	9.1
Vicibactin	775.3732		$C_{33}H_{54}N_6O_{15}$	9.0

Table S3. List of m/z corresponding to positive matches identified for Fe(III) complexes, as well as m/z of found potential apo forms (at m/z 52.991Th lower), and proposed molecular formula in those cases in which it was possible to assign a formula matching the isotope pattern and below the mass error threshold of 3 ppm.

Elution time (min)	$[M-2H+^{56}Fe]^+$ *m/z*	$[M+H]^+$ *m/z*	Proposed Molecular formula
4.2	413.8703		
4.2	628.8559		
4.6	518.7773		
5.3	1159.3507	1106.4407	$C_{24}H_{68}FeO_{13}N_{27}S_5$
5.4	546.7157		
6.0	614.1271	561.2150	$C_{21}H_{30}O_{12}N_6Fe$
7.2	580.6707		
8.6	517.2899		
8.7	509.7859		
8.8	428.2495		
8.8	547.2993		
8.8	616.3672		
8.8	678.3465		
8.9	549.3145		
8.9	591.3505		
8.9	847.4677		
9.0	576.3246		
9.0	702.4151		
9.0	885.5463		
9.0	890.4263	837.5144	
9.1	474.2826		
9.1	506.3087		
9.1	609.1521	556.2404	
9.1	781.2316	728.3230	$C_{43}H_{48}FeO_6S_2$
9.2	463.2558		
9.2	556.2875		
9.2	918.4899		
9.2	918.4899		
9.3	433.2450		
9.3	444.2250		
9.3	743.4100		
9.4	362.2080		$C_{13}H_{33}O_2N_6Fe$
9.4	593.3442		
9.4	1027.5127		
9.7	415.2346		
9.7	486.2717		
9.7	752.3984		
9.7	760.4249		
9.8	528.3186		

Table S3. (Cont.)

Elution time (min)	$[M-2H+^{56}Fe]^+$ *m/z*	$[M+H]^+$ *m/z*	Proposed Molecular formula
9.8	574.3602		
9.8	606.3326		
9.9	592.3712		
10.0	685.4290		
10.3	684.1790		$C_{23}H_{40}FeN_4O_{16}$
10.4	781.2331		
11.2	453.1887		
11.6	917.2481		
11.7	912.2270		$C_{36}H_{56}O_8N_6FeP_5$
12.0	903.2322		
12.3	506.1041		
12.3	616.1770		
13.0	804.3187		$C_{30}H_{54}O_{13}N_9Fe$

Table S4. List of m/z corresponding to positive matches identified for Cu(II) complexes, and the matched isotopes observed in the pattern.

Elution time (min)	$[M\text{-}H+^{65}Cu]^+$ *m/z*	Matched isotopes
4.8	558.8005	3
4.8	574.7847	2
4.8	716.6904	3
4.8	780.9684	3
4.8	874.6899	3
4.9	802.9382	3
5.4	1275.3396	2
5.5	616.1260	4
5.5	634.1359	3
5.5	1161.3511	3
5.5	1663.5365	3
6.5	919.3032	5
6.5	935.1985	2
8.8	607.1028	4
8.8	644.3552	3
9.0	643.3963	3
9.2	474.2179	3
9.2	523.3068	3
9.2	684.3674	3
9.3	531.3317	4
9.3	565.3541	3
9.7	532.2597	4
9.7	672.3437	3
11.1	903.3088	4
11.5	1005.3507	3

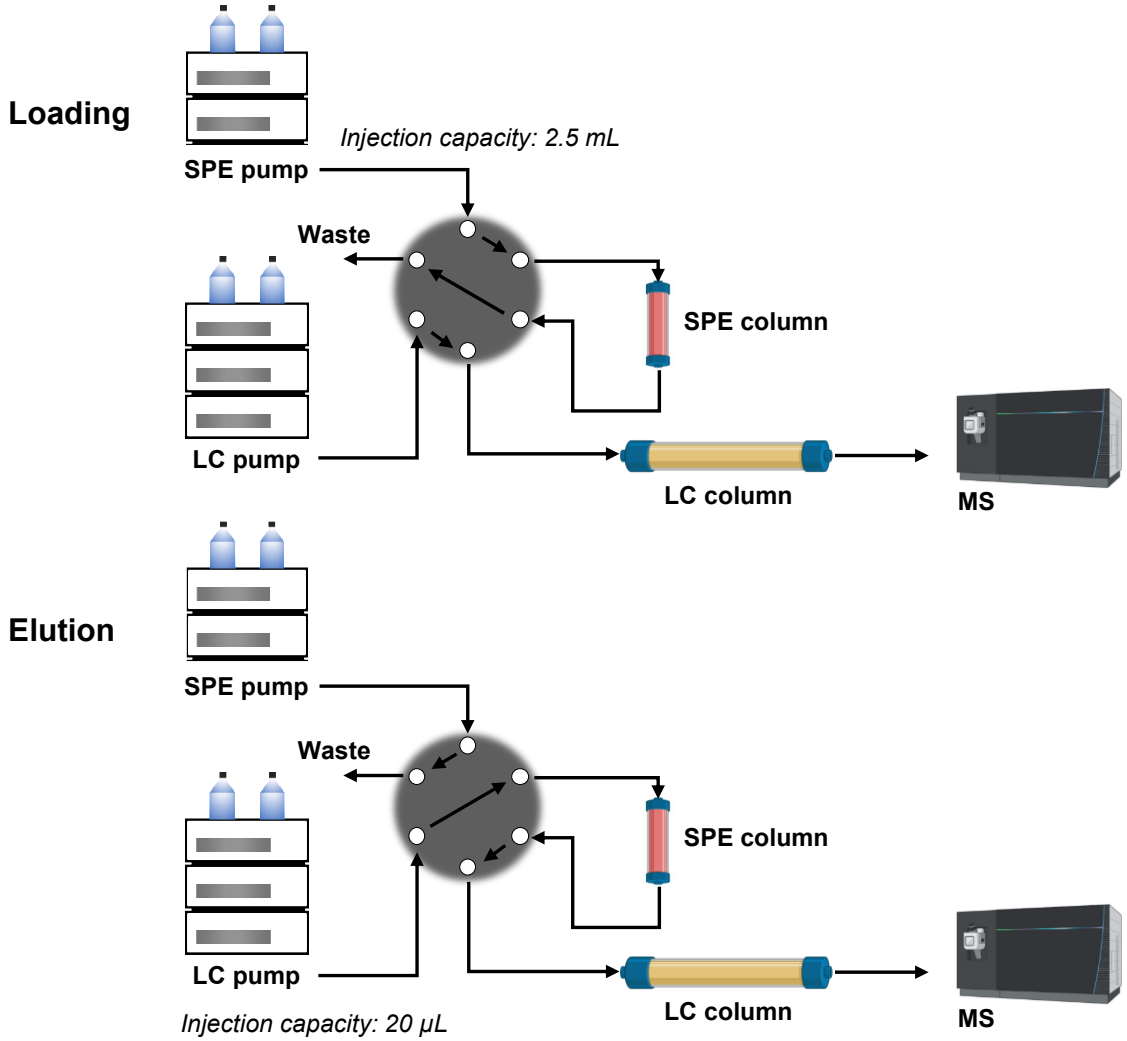

Figure S1. Schematic representation of online SPE. During the loading phase, siderophores in the injected sample are retained in the SPE column, whereas all hydrophilic and salts in the sample are washed out. After switching the valve to the elution position, the gradient from the LC column elutes the siderophores from the SPE column to be then separated chromatographically with the LC column under gradient conditions.

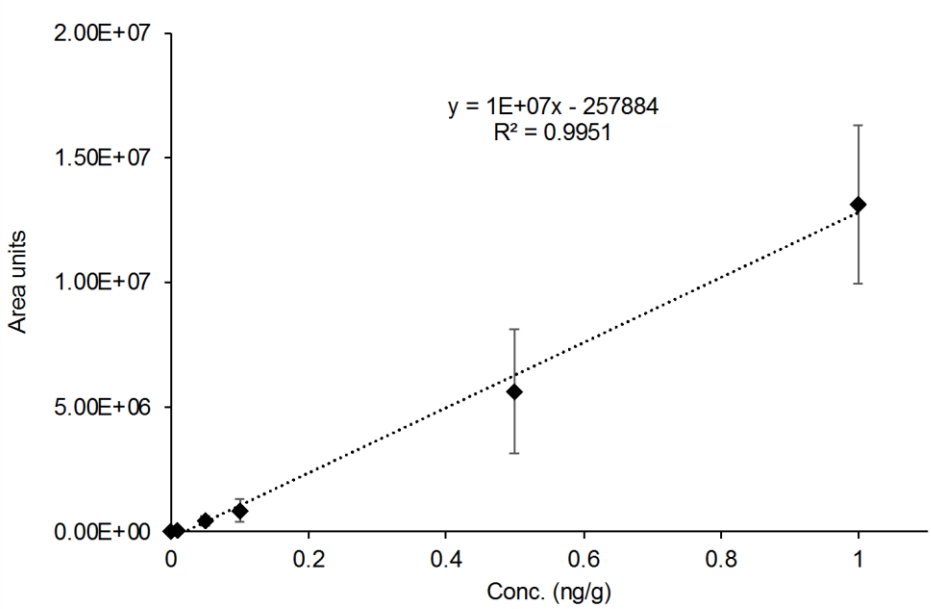

Figure S2. Calibration curve obtained by averaging the area obtained for the siderophores standards.

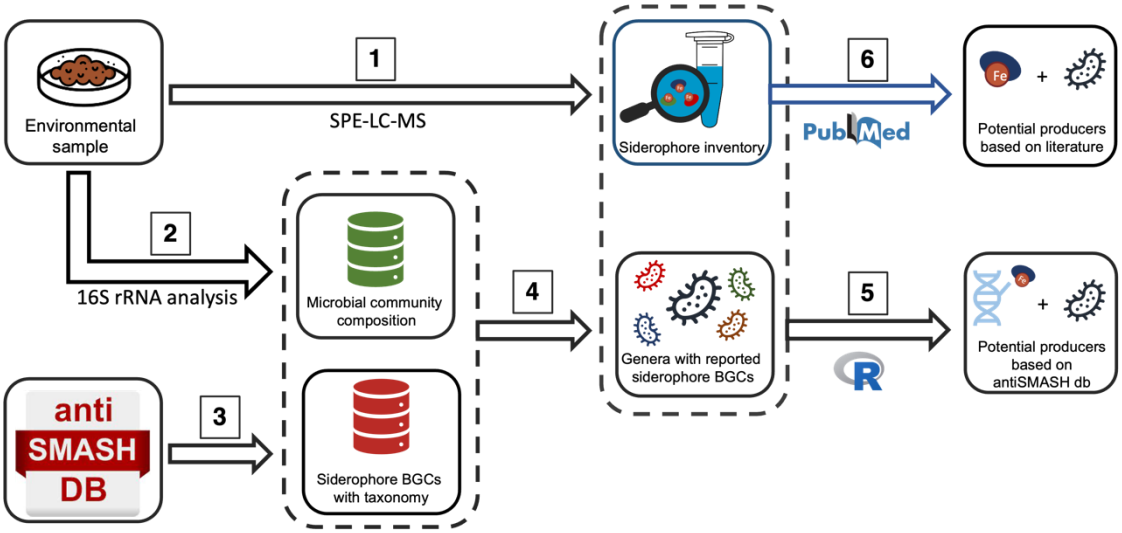

Figure S3. Main steps of the taxonomic-based inference method proposed for fast-screening of potential siderophore producers in environmental samples. Environmental sample is processed to obtain 1) an inventory of siderophores using SPE-LC-MS and 2) the taxonomic composition at the genus level of the microbial community. Next steps included: 3) retrieval of the siderophore database from antiSMASH Biosynthetic Gene Cluster database (DB; https://antismash-db.secondarymetabolites.org); 4) antiSMASH siderophore database filtering against the microorganisms detected to retrieve all siderophores producer candidates; 5) Specific association of the siderophores identified in the sample to a potential producer. In parallel, 6) Known microbial producers for the siderophores detected were searched in the literature. This information is then crossed with the microorganisms identified in the sample.

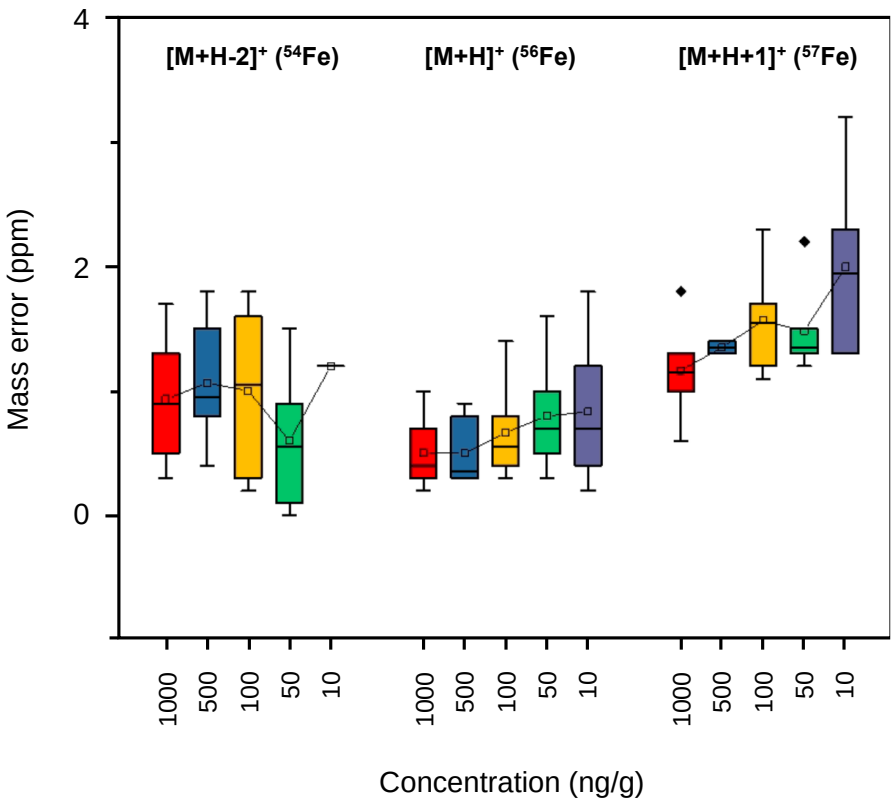

Figure S4. Mass error of MS isotopologues of ferryl standards at different concentration ranges.

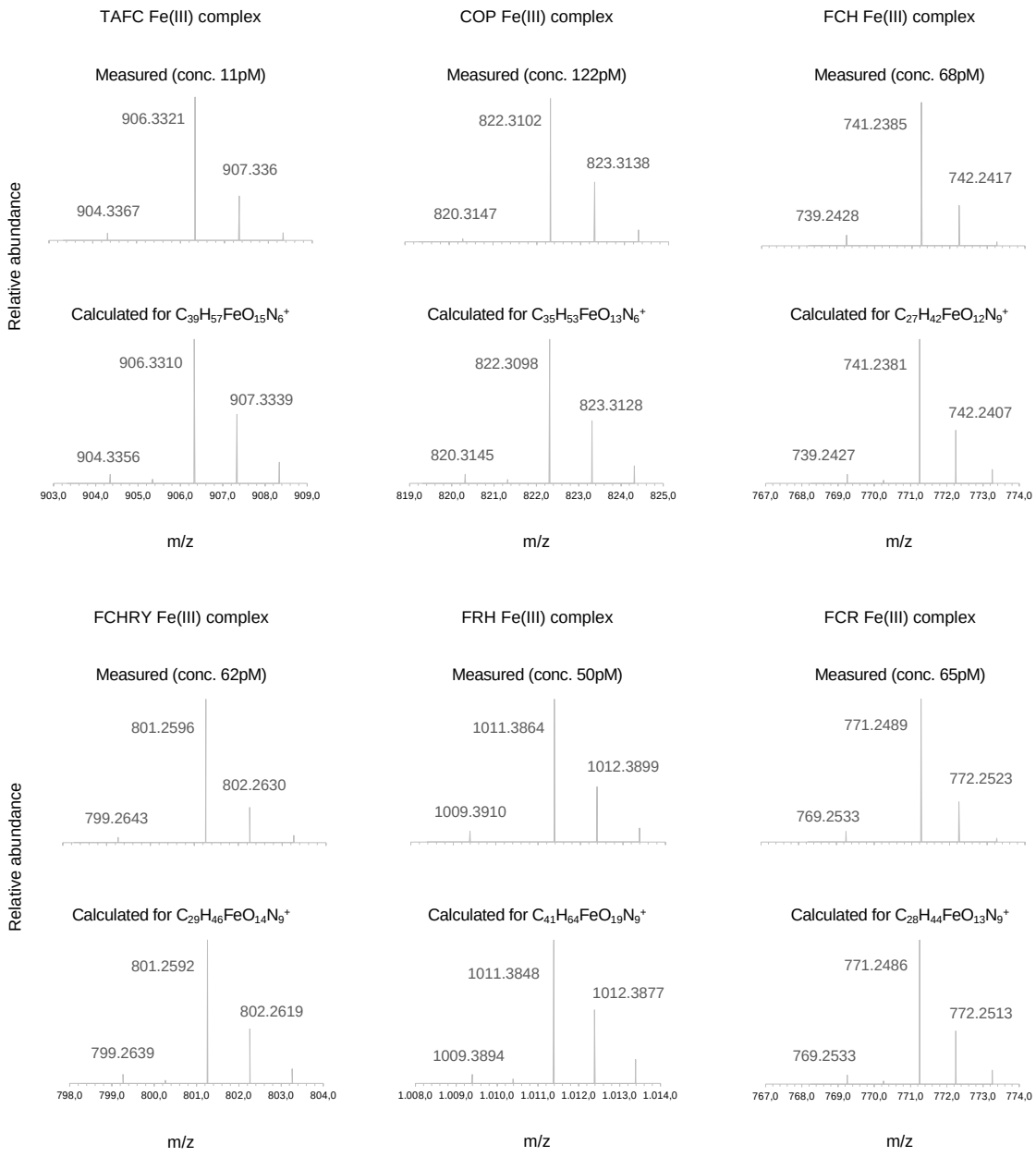

Figure S5. Comparison of theoretical and experimentally obtained MS isotope pattern for siderophores standards Triacetylfusarinine C (TAFC), Coprogen (COP), Ferrichrome (FCH), Ferrichrysin (FCHRY), Ferricrocin (FCR), and Ferrirhodin (FRH).

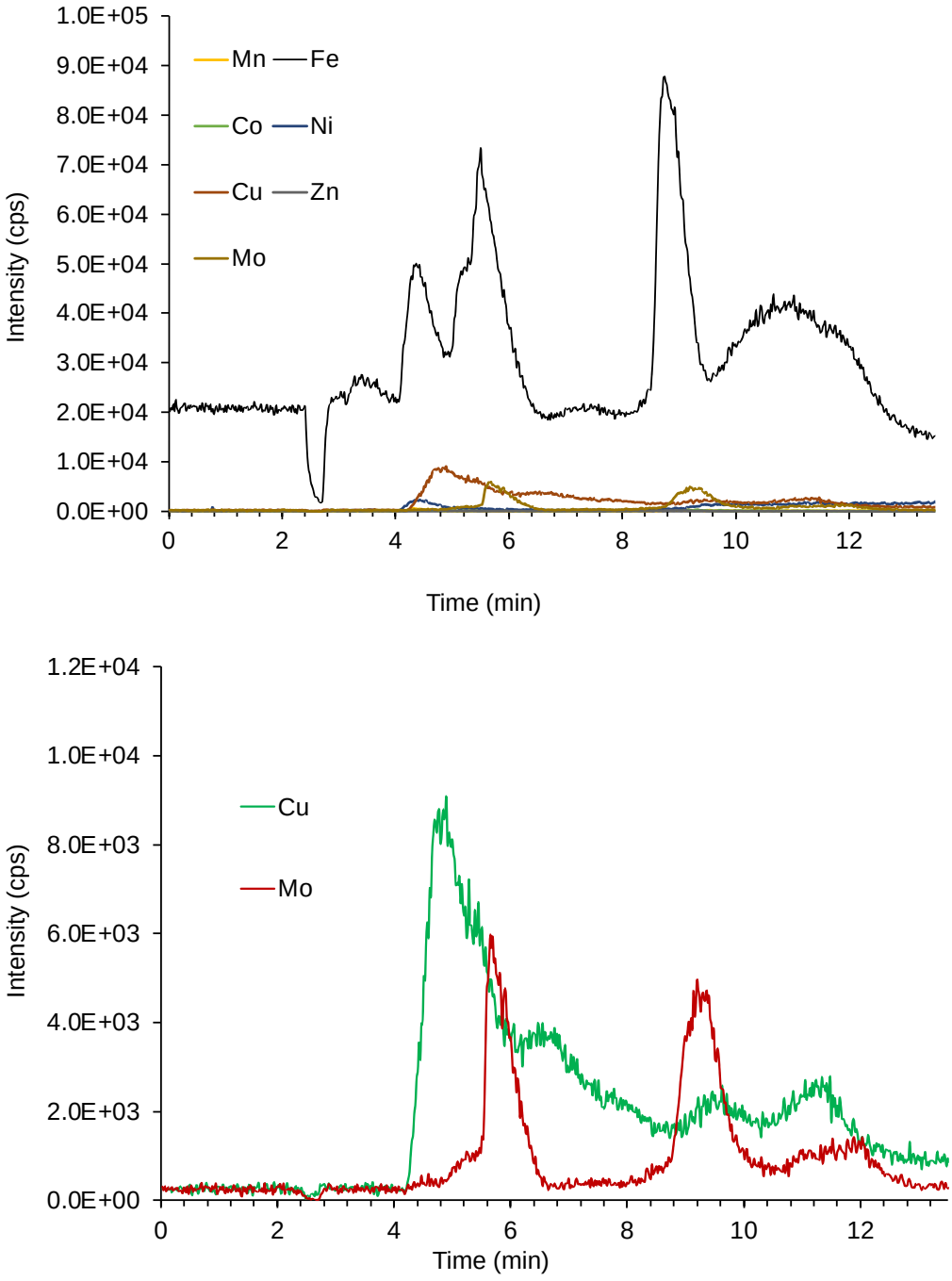

Figure S6. SPE-RP-ICP-MS chromatograms of Bernadouze peatland sample monitoring Mn, Co, Cu, Mo, Fe, Ni and Zn signals. The chromatogram below shows rescaled Mo and Cu signals.

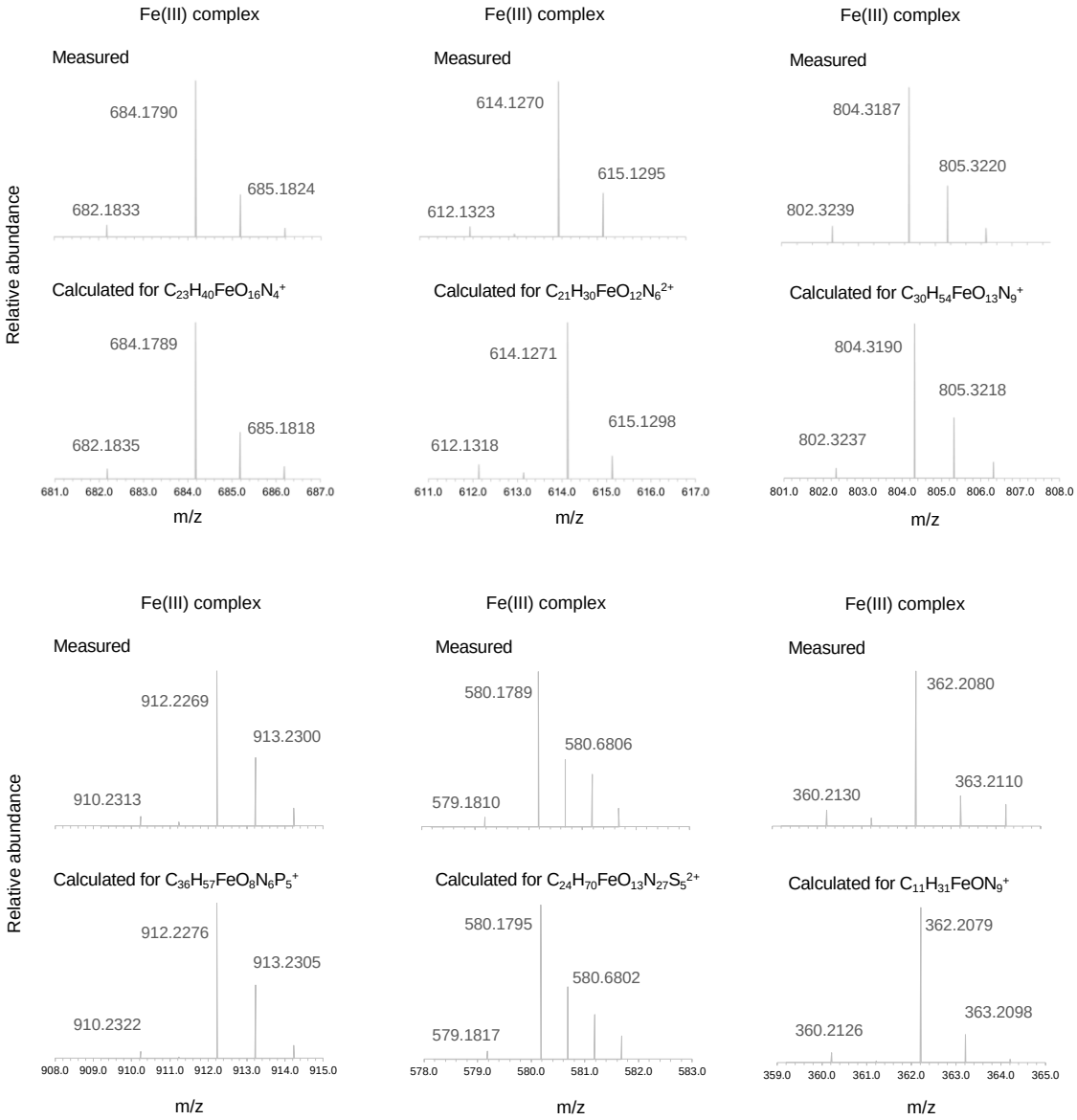

Figure S7. Comparison of theoretical and experimentally obtained MS isotope pattern for potential metal complexes identified in Bernadouze sample SPE-LC-MS analysis.

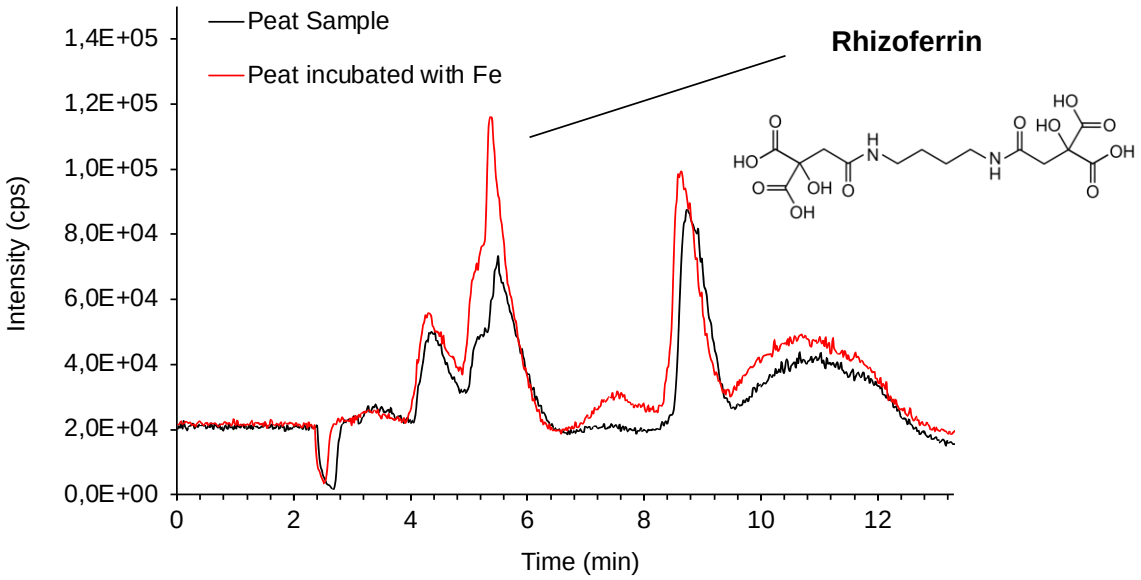

Figure S8. SPE-LC-ICP-MS chromatogram monitoring iron signal, corresponding to peat sample (black), and peat sample incubated with iron excess. Iron was spiked as iron citrate, at 5nM concentration, which is estimated to be 5 times higher than total metallophores concentration. Only in the peak at Rt around 6 min we can observe significant increase in iron signal. This Rt corresponds to Rhizoferrin retention time, which agrees with observations in Fig S9.

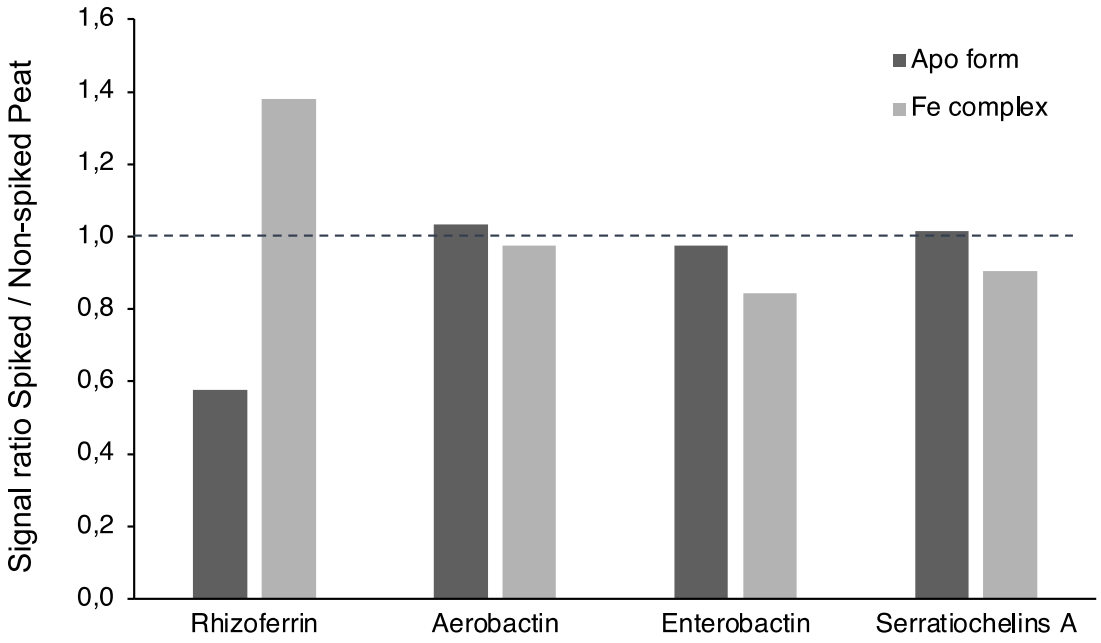

Figure S9. Signal ratio of apo and ferryl form of most abundant siderophores identified in Bernadouze peatland rhizoferric, aerobactin, enterobactin and serratiochelins A, when the peat sample was spiked with excess of Fe, against the direct "native" sample. The most significant change occurs in the case of rhizoferrin, in which an increase of the complexation with Fe is observed. In the case of enterobactin and serratiochelins (and aerobactin less significantly), the opposite effect is observed. There is a decrease in the proportion of ferryl form. There has been reported that the excess of Fe^{3+} can lead to the formation of iron oxide colloids even at low pH, which in turn can lead to the reduction of MS signal of siderophores.[1] That effect is evidence that metal incubation is ought to alter the natural environment of the sample.

References

(1) Rai, V.; Fisher, N.; Duckworth, O. W.; Baars, O. Extraction and Detection of Structurally Diverse Siderophores in Soil. *Front Microbiol* **2020**, *11*, 2165. https://doi.org/10.3389/FMICB.2020.581508/BIBTEX.